NASA TECHNICAL NOTE

NASA TN D-3795

EXPERIMENTAL INVESTIGATION OF
SECONDARY JETS FROM TWO-DIMENSIONAL
NOZZLES WITH VARIOUS EXIT MACH NUMBERS
FOR HYPERSONIC CONTROL APPLICATION

by James R. Sterrett, John B. Barber, Daisy W. Alston,
and David J. Romeo

Langley Research Center
Langley Station, Hampton, Va.

EXPERIMENTAL INVESTIGATION OF SECONDARY JETS FROM

TWO-DIMENSIONAL NOZZLES WITH VARIOUS EXIT MACH NUMBERS

FOR HYPERSONIC CONTROL APPLICATION

By James R. Sterrett, John B. Barber, Daisy W. Alston,
and David J. Romeo

Langley Research Center
Langley Station, Hampton, Va.

EXPERIMENTAL INVESTIGATION OF SECONDARY JETS FROM

TWO-DIMENSIONAL NOZZLES WITH VARIOUS EXIT MACH NUMBERS

FOR HYPERSONIC CONTROL APPLICATION

By James R. Sterrett, John B. Barber, Daisy W. Alston,
and David J. Romeo
Langley Research Center

SUMMARY

The effects of two-dimensional secondary jets issuing approximately perpendicular to a flat plate have been investigated at a free-stream Mach number of 6. The parameters varied were secondary jet exit Mach number (1 to 6), jet total pressure, and jet orifice width. Free-stream tunnel conditions and secondary jet total temperatures remained constant. The boundary layer on the plate in the vicinity of the jet was turbulent. In addition to jet shock structures, jet penetration, and separation distances, the gross aerodynamic normal forces as determined from pressure distributions were examined. The magnitude of the surface pressures ahead of the jet exit position can be largely determined from boundary-layer separation considerations. However, the extent of the separation region is determined by the jet penetration height, an indication of which was obtained from measurements of the jet strong-shock standoff distance from the plate surface. The separation distances, jet strong-shock standoff distances, and aerodynamic normal forces for the sonic jet with various slot widths can be correlated with the use of a parameter which for this investigation is proportional to the jet mass flow (and the jet momentum). The ratio of the aerodynamic normal-force coefficient to the reaction normal-force coefficient increases with decreasing jet mass flow (and jet momentum). Therefore, the force ratio will increase as either slot width or jet total pressure is decreased. However, the force ratio remains approximately constant for any given jet mass flow (or jet momentum) regardless of slot width or jet pressure ratio. For the sonic jets, the force ratio varied from approximately 1.7 to 0.8. The data for the conditions of this investigation show that the aerodynamic normal force for a given jet mass flow decreases with increasing jet exit Mach number but the total normal force (including reaction) is a constant for a given jet mass flow and independent of jet exit Mach number.

INTRODUCTION

The study of the interaction of secondary gaseous jets with a hypersonic primary stream is of interest as a means of aerodynamic control for hypersonic vehicles, for

thrust vector controls in rocket nozzles, and for fluid amplification. A number of experimental and analytical investigations on this subject have been published; among them are references 1 to 10. References 4 and 6 report results of tests of secondary injection from flat plates and references 1, 2, 6, 7, and 8 report results of secondary injection from cylindrical bodies. References 1, 2, 3, 5, 9, and 10 present various theoretical analyses of the problem. Although results from these investigations add to the general knowledge of secondary jets, the interaction processes are still not well understood. Two things which would aid in the development of a better theoretical approach are a better knowledge of the secondary jet structure (including the interaction process between the jet and the mainstream) and additional quantitative information concerning the importance of various parameters as determined experimentally.

The approach to the problem of determining the flow process was to conduct both experimental and theoretical investigations. The experimental phase of the program consisted of an investigation of free jets exhausting against a flat plate and an investigation conducted in the Langley 20-inch hypersonic Mach 6 tunnel with secondary jets issuing perpendicularly from a flat plate. The theoretical investigation included the layout of various free jet patterns by the use of the two-dimensional characteristic theory for various boundary conditions and the examination of various shock calculations for different shock patterns. The purpose of this paper is to present the results of the investigation conducted in the wind tunnel; however, some results from the other part of the study (which are partially reported in ref. 11) are stated for clarity.

Specifically, this paper presents the results obtained by injecting air from two-dimensional slots located near the rear of a two-dimensional flat plate into a Mach 6 primary stream. The parameters varied were secondary jet exit Mach number (1 to 6), slot width, jet total pressure, and end plates for the model. In addition to jet shock structure, jet penetration, and separation distances, the gross aerodynamic normal forces as determined from pressure distributions were examined. The experiments were conducted with a boundary-layer trip and with a free-stream unit Reynolds number of 6.5×10^6 per foot (21.3×10^6 per meter) which insured a turbulent boundary layer on the section of the plate where the interaction between the jet and the primary stream occurred.

SYMBOLS

a sonic velocity, feet per second   (meters per second)

b slot span, inches   (meters)

$c_{N,A}$ coefficient of integrated normal force per inch span due to aerodynamic interaction of jet, $F_{N,A}/qL$

$c_{N,R}$ coefficient of calculated normal force per inch span due to reaction of jet alone, $F_{N,R}/qL$

d width of jet slot at throat, inches (meters)

$F_{N,A}$ integrated normal force per inch span due to aerodynamic interaction of jet, $\int_{l} (p - p_o)dx$, pounds per inch (newtons per meter)

$F_{N,R}$ calculated normal force per inch span due to reaction of jet alone,

$$\frac{d}{M_j}\left[\frac{2 + (\gamma - 1)M_j^2}{\gamma + 1}\right]^{\frac{\gamma+1}{2\gamma-2}}\left[\left(\frac{2}{2 + (\gamma - 1)M_j^2}\right)^{\frac{\gamma}{\gamma-1}}\left(M_j^2\gamma + 1\right)p_{t,j} - p_o\right], \text{ pounds per}$$

inch (newtons per meter)

h height of jet strong shock, measured vertically from plate, inches (meters)

J jet momentum, (see eq. (3))

K, K_1, K_2, K_3 constant

L length of plate, inches (meters)

l length of separated region, inches (meters)

M Mach number

$\dot{m}$ mass flow rate of jet per inch span, slugs/second-inch (kilograms per second-meter) (see eq. (1))

p pressure, pounds per inch^2 absolute (newtons per meter^2)

q dynamic pressure, pounds per inch^2 absolute (newtons per meter^2)

R Reynolds number

T temperature, $^\circ R$ ($^\circ K$)

T_w wall temperature, $^\circ R$ ($^\circ K$)

u	velocity
x	lengthwise distance along plate measured from jet, positive forward, inches (meters)
y	perpendicular distance above plate, inches (meters)
γ	ratio of specific heats, assumed to be 1.4 for jets
δ^*	boundary-layer displacement thickness
μ	viscosity
ρ	density, slugs per foot^3 (kilograms per meter^3)

Subscripts:

j	jet exit conditions
o	local conditions on plate with attached flow
p1	conditions at first peak pressure for turbulent separation
p2	conditions at second peak pressure for turbulent separation
t,j	jet stagnation conditions
t,∞	primary stream stagnation conditions
∞	free-stream test-section conditions

APPARATUS AND TEST METHODS

Wind Tunnel

This program was carried out in the Langley 20-inch hypersonic Mach 6 tunnel. This tunnel is a blowdown type and was operated at a stagnation pressure of approximately 23.1 atm (1 atm = 101 325 N/m^2) and at a stagnation temperature of 400° F (478° K). The corresponding Reynolds number was approximately 6.5×10^6 per foot (21.3×10^6 per meter). A more complete description of the tunnel is given in reference 12.

4

Models and Support

The basic model used in this program was a flat plate (fig. 1) with a 10-in. (25 cm) span and a 10° leading edge that tapered to a maximum radius of 0.001 in. (0.02 mm). The distance from the jet slot to the leading edge of the plate was 19.25 in. (48.89 cm). A boundary-layer trip, consisting of 1/16-in. (1.59 mm) set screws projecting 1/8 in. (3.18 mm) above the plate and at 3/8 in. (9.54 mm) centers, was located 1.5 in. (3.8 cm) from the leading edge. Twenty-eight 0.06-in-diameter (1.5 mm) pressure orifices were installed along the center line of the plate, to measure surface pressures in the jet induced separation region.

The jets, two dimensional, were formed by the back of the flat plate and interchangeable nozzle pieces. The sonic nozzle was adjustable, by means of inserting shims between the nozzle and flat plate at the ends of the jet slot. This allowed variation of the jet slot throat width from 0.005 in. (0.13 mm) to 0.054 in. (1.37 mm). Figure 1(c) shows a sketch of the sonic nozzle. The jet slot had a span of 8 in. (20 cm).

Supersonic nozzles were contoured for a perfect gas of $\gamma = 1.4$ and did not have adjustable throat widths. Five different supersonic nozzles were employed: one Mach 2.0, two Mach 3.2, one Mach 4.0, and one Mach 6.2. The throat widths of the Mach 2.0, one of the 3.2, and the 4.0 nozzles were nominally 0.02 in. (0.5 mm). The Mach 6.2 nozzle, however, would have had relatively a very large exit width with that throat size, so it was constructed with a 0.01-in. (0.2 mm) throat instead. Accordingly, the second Mach 3.2 nozzle also had a 0.01-in. (0.2 mm) throat to allow correlation of data from the Mach 6.2 nozzle with that of the other nozzles. A sketch of the Mach 6.2 nozzle mounted on the plate is shown in figure 1(a), the Mach 6.2 nozzle is shown in figure 1(b), and a typical supersonic nozzle is shown in figure 1(d).

Several runs were made, with the sonic nozzle, using side plates on the model (fig. 1(e)) to determine if three-dimensional effects were significant along the center line of the plate. Nozzle throats used varied again from 0.005 in. (0.18 mm) to 0.054 in. (1.37 mm).

Room temperature dry air for the jets was supplied to the model through a pipe at the rear of the plate. It then passed into a settling chamber and on through the nozzle. This airflow was controlled by a hand-operated valve.

The top surface of the nozzles was fitted with a 0.06-in-diameter (1.5 mm) pressure orifice. This, and a removable backpiece fitted with five more pressure orifices of this size, permitted pressure measurements on the top surface of an extension of the plate in the back of the jet. (See fig. 1(f).)

The model was rigidly mounted in the wind tunnel, flat plate surface facing downward, and supported by two struts mounted at about the middle of the plate and by the jet air supply pipe.

The jet total pressure was measured by a 0- to 34-atmosphere transducer, and plate surface pressures were measured by 0- to 0.34-atmosphere transducers. Data were recorded by means of a commercial digital readout system on magnetic tape. All measurements were made after allowing time for the model to achieve an approximately constant temperature. Plate pressures were recorded for incremental changes in jet total pressure for the various supersonic nozzles. In addition, schlieren photographs were taken at many test conditions to study the interaction phenomena visually.

Previous heat-transfer measurements taken in this same tunnel on a flat plate without a boundary-layer trip have shown that turbulent flow began at approximately a Reynolds number of 5×10^6 for conditions similar to the present tests. To increase the extent of the turbulent flow, boundary-layer trips with heights sufficient to move turbulent flow to the vicinity of the trip (ref. 13) were added to the plate for the present tests. Although boundary-layer profiles were not taken for the present test conditions, boundary-layer surveys were available which were taken on the plate with the same roughness configuration as for the present tests and under conditions where the free-stream Reynolds number was 26.2 percent higher than the present tests. The velocity profiles were obtained from local pitot-pressure measurements and stagnation temperatures calculated from the Crocco energy equation in conjunction with the conventional assumption of constant static pressure through the boundary layer. Velocity profiles calculated from these surveys at two positions on the plate are presented in figure 2. These profiles are as expected for a turbulent boundary layer.

The nozzle throat widths tended to enlarge with increasing jet total pressure. This enlargement was nominally independent of the initial jet throat width for a given nozzle, although it did vary among different nozzles. Although the enlargement was insignificant for the larger throat widths, it was a sizable percentage of the smaller (as high as approximately 28 percent for $d = 0.007$ in. (0.018 cm) for the sonic nozzle). In order to obtain a calibration for this enlargement, each jet configuration was exhausted into still air and the deviation measured by a mechanical dial indicator both before and after each test run. These deviation measurements were used to correct the nominal values of jet throat width d. The corrected values were then used wherever the quantity d appeared explicitly in a parameter or calculation. In general plots of data for various jet throat widths, however, the data are grouped by their nominal throat width values. Interference between the wind-tunnel surface and the jet-deflected primary stream was believed to have no effect on the data, inasmuch as the tests were made with the plate at two different vertical positions in the tunnel and no differences in the data for otherwise identical test conditions were noted.

6

RESULTS AND DISCUSSION

Characteristic of Flow Field

Flow model.- When the flow from a secondary jet issues into a supersonic or hypersonic primary stream, it produces a very complex flow field. Although it is difficult to describe the flow in minute detail, reference 11 indicates that the gross aerodynamic structure of the flow can be established from considerations of free jets and the inspection of schlieren photographs taken of secondary jets exhausting into a primary stream. A sketch which shows the characteristics of a jet is shown in figure 3. Although this sketch is for a jet exhausting into a partially evacuated chamber where it is assumed that the pressure on the two sides of the jet are different, the same general patterns exist for a secondary jet exhausting approximately perpendicular to the primary stream. In general, experimental data have shown that the pressures on the upstream and downstream sides of a secondary jet are different. For a given gas the jet total pressure and the exterior pressures in regions A and B of figure 3 determine the position of the side boundaries and the internal shocks on sides A and B, respectively.

The schlieren photographs of figures 4 and 5 are typical of flow patterns often observed when a secondary jet interacts with the primary flow. A sketch of the envisioned flow field (ref. 11), differing somewhat from that usually shown, is given in figure 4(c). Part of the fluid turns in an upstream direction and somewhere forms a mutual stagnation point with the flow coming in the opposite direction. As drawn, the dividing boundary indicates that the flow from the jet penetrates the upstream separated region somewhat similar to the usual cavity or wake flow separation model with mass injection. (E.g., see ref. 14.) However, the exact location of the dividing boundary has not been established. Of special interest are the separation regions upstream and downstream of the secondary jet and the distance that the secondary jet penetrates into the primary stream. The effect of various design parameters on conditions in these regions is discussed in the following section.

Choice of correlating parameter.- Considerable thought has been given by various investigators to a proper choice of parameter for correlation of secondary injection performance characteristics (e.g., refs. 1, 5, and 6). However, the validity of the choice of physical quantities which are relevant to the phenomena is not definitely established. When reasoning similar to that of reference 1 is used, the interaction characteristics are expected to be functions of $p_{t,\infty}$, $\rho_{t,\infty}$, μ_∞, γ_∞, M_∞, $p_{t,j}$, $\rho_{t,j}$, μ_j, γ_j, d, M_j, b, and L (somewhat arbitrarily chosen to be a characteristic length parameter). Because of the experimental conditions of these investigations (e.g., constant wind-tunnel conditions), several of these quantities can be eliminated from the list of variables and with dimensional analysis similar to that of reference 1 the remaining can be arranged

in the following nondimensional forms: $p_{t,j}/p_{t,\infty}$, d/L, M_j, and $\rho_{t,j}/\rho_{t,\infty}$. As pointed out in reference 1, other combinations of dimensionless parameters can be formed. However, they can also be derived from this last grouping if the original list of physical quantities is assumed to be complete. Two commonly used correlating parameters are $p_{t,j}/p_{t,\infty}$ and $\left(p_{t,j}/p_{t,\infty}\right)(d/L)$. This latter one is an indication of the jet mass flow per unit span since when the injectant is air and $p_{t,\infty}$ and $T_{t,j}$ are constant, as in this investigation:

$$\dot{m} = \frac{0.01652 p_{t,j} d}{\sqrt{T_{t,j}}} \frac{p_{t,\infty}}{p_{t,\infty}} \frac{L}{L} = \frac{p_{t,j}}{p_{t,\infty}} \frac{d}{L} K \tag{1}$$

In addition, a jet momentum parameter J can be obtained from a combination of all the nondimensional quantities since

$$\dot{m} u_j = \dot{m} M_j a_j = f\left(p_{t,j}, \rho_{t,j}, M_j, d\right) \tag{2}$$

As can be seen from equation (2), since the jets have a constant total temperature for this investigation the jet momentum is proportional to the jet mass flow for a given value of M_j, the relationship between jet momentum and $\left(p_{t,j}/p_{t,\infty}\right)(d/L)$ being

$$J = \left[\frac{p_{t,j}}{p_{t,\infty}} \frac{d}{L}\right]\left[K M_j a_j\right] \tag{3}$$

where the quantity in the second brackets is constant for a given jet Mach number. In the present report, the parameter $\left(p_{t,j}/p_{t,\infty}\right)(d/L)$ is generally used as the correlating parameter since it most successfully correlates the results obtained from these tests.

Surface pressure distributions.- The schlieren photograph shown in figure 5 along with the pressure distribution illustrates the position relationship between the flow patterns and the various pressure regions defined in that figure. This photograph also supports the belief that interference between the tunnel surface and the jet-deflected primary stream did not affect the data. The first peak pressure region is characteristic of that observed in a turbulent separation region. (See refs. 12 and 15 for pressure distributions in a separated region where separation was forced by the forward-facing step.) It is postulated that the second and third peak pressures are associated with the reverse flow of the jet and primary stream separation as indicated by the sketch of figure 4(c). (Visual observations indicate that the flow patterns are relatively stationary; however, high-speed photography shows that the flow patterns fluctuate slightly with time.)

Figures 6 and 7 present typical examples of the chordwise pressure distributions on the center line ahead of the jet position for varying jet total pressure (side plates were not used for these tests). Increasing the total pressure ratio for any particular slot for

8

.a sonic jet causes a growth in the extent of these separation regions within the present range of test conditions (fig. 6); however, the trends of the pressure distributions remain similar for all slot widths (fig. 7) and total pressure ratios. However, at the very small total pressure ratios, the regions of separation are so small that the second and third peak pressure regions are not easily discernible. Typical examples of pressure distributions obtained when side plates were used are shown in figure 8, compared with identical cases without the side plates. The side plates were used to investigate the effect on surface pressure of leakage over the sides of the model of air from the separated region. The shape of the pressure distributions for both conditions is similar; however, the influence of the jet is felt a little further forward for the model with side plates. The effect of this on aerodynamic interaction forces is discussed in the section "Aerodynamic Interaction Forces."

An inspection of figures 9 to 13 which present pressure distributions for various jet exit Mach numbers also shows similar trends to those observed with a sonic jet. A comparison of the pressure distributions for various exit Mach number jets at approximately the same total pressure ratio is shown in figure 13. The slot widths of the supersonic jets are approximately 0.020 in. (0.51 mm). For the conditions of these tests, the area of influence ahead of the jet position decreases with increasing exit Mach number when all other parameters remain constant.

A plot which shows the first peak pressures for various slot widths and jet exit Mach numbers is presented in figure 14. The peak pressures are reasonably well correlated when plotted as a function of the parameter $\left(p_{t,j}/p_{t,\infty}\right)(d/L)$. Previous investigations with various step heights have shown that for turbulent flow the first peak pressure in the separation region increases with step height (increasing penetration into the stream) until the step height becomes sufficiently large and the first peak pressure then becomes only a very weak function of increased step height and Reynolds number. The figure shows that, for the present test conditions, the first peak pressures are essentially independent of jet exit Mach number but increase slightly when the parameter $\left(p_{t,j}/p_{t,\infty}\right)(d/L)$ is increased. The first peak pressures are approximated by the equation of reference 12 which gives the first peak pressures for a forward-facing step which is larger than the boundary-layer thickness. Similarly, a plot of the second peak pressures is shown in figure 15, where it can be seen that the peak pressures are reasonably well correlated when plotted against the parameter $\left(p_{t,j}/p_{t,\infty}\right)(d/L)$.

The surface pressures downstream of the secondary jet (fig. 16) are generally less than free-stream conditions. In general, the downstream surface pressures decrease as the total pressure ratio increases; however, the pressures appear to be leveling off at the higher total pressure ratios. The variation or trend of surface pressures with distance from the slot location changes with total pressure ratio. This is probably caused by the

change with jet total pressure of the location of the reattachment shock and the separation vortex sketched in figure 4.

Separation distances and height of jet strong shock.- Presented in figure 17 is a plot of the separation distances due to the jet determined from schlieren photographs and pressure distributions. The parameter $\left(p_{t,j}/p_{t,\infty}\right)(d/L)$ successfully correlates the length of the separated region for all slot widths and jet pressures. At the lower values the effect of this parameter on l is stronger than at higher values. Length of the separated region was taken as the distance from the upstream nozzle wall of the jet to the point where the pressure on the plate surface was nominally equal to the surface pressure without the jet. (See fig. 5.) It was found from schlieren photographs that the separation point as determined from pressure distributions coincided with the point of the impingement of the separation shock, if extended, on the plate. Previous work (ref. 12) has shown, by film techniques, that the actual point of separation lies slightly farther downstream from the position used in the present investigation and occurred at a position about halfway up the leading pressure rise. No such techniques were used; however, the method used for determining a "hypothetical" separation point from the pressure distributions and schlieren photographs fits the purpose of this report adequately.

The jet strong shock heights were measured from schlieren photographs of the flow. Figure 18 shows the correlation of the height of the jet strong shock. The parameter $\left(p_{t,j}/p_{t,\infty}\right)(d/L)$ successfully correlates the shock height for all jet slot widths and jet pressures. By comparing this figure with figure 17, the plot of separation distance against the same parameter, the two curves are seen to be similar. Intuitively, this might be expected since the separation angle for turbulent separation is nearly a constant for a given free-stream Mach number, and separation lengths are nominally proportional, by geometry, to the height of the disturbance. The height of the jet strong shock is an indication of this disturbance height. An actual measurement of the height of the disturbance, the height of jet penetration into the primary stream, is impossible because the contact surface between the two flows cannot be ascertained from the schlieren photographs.

The large spread in the data of figure 18 is due to difficulty in measuring the exact height of the shock from the photographs. Due to possible three-dimensional effects on the ends of the jet, turbulence in the flow, and optical effects, the shock appeared as a band instead of a thin line. For each case, the height from the plate to the top and bottom of the band was measured and plotted.

Aerodynamic Interaction Forces

Sonic jets.- Aerodynamic normal forces due to the interaction between a sonic jet and primary flow over the plate were obtained by mechanical integration of the plate

•pressure distribution curves. These forces were calculated ahead of the jet only, and the results do not include the effects of the low pressure region behind the jet where the pressures are generally less than primary stream conditions. Also, the pressures used to determine these forces were obtained along the center line of the plate and therefore do not include the three-dimensional effects occurring near the plate edges.

Figure 19 shows the aerodynamic normal forces in coefficient form plotted against the parameter $\left(p_{t,j}/p_{t,\infty}\right)(d/L)$. Also in this figure the jet reaction force coefficient is plotted. An inspection of figures 17, 18, and 19 shows a similarity between the plots of h/L against $\left(p_{t,j}/p_{t,\infty}\right)(d/L)$, l/L against $\left(p_{t,j}/p_{t,\infty}\right)(d/L)$, and $C_{N,A}$ against $\left(p_{t,j}/p_{t,\infty}\right)(d/L)$. This similarity is further illustrated by plotting together h/L, l/L, and $C_{N,A}$ on a logarithmic scale as in figure 20. As can be seen from this figure, on logarithmic scales the curves of h/L, l/L, and $C_{N,A}$ are nominally straight-line functions of the jet mass flow parameter. Also, their slopes are approximately equal although the slope of the $C_{N,A}$ curve appears a little greater than that of h/L and l/L. Therefore, for the present data the following relations may be written:

$$\frac{h}{L} = K_1 \left(\frac{p_{t,j}d}{p_{t,\infty}L}\right)^a \tag{4}$$

$$\frac{l}{L} = K_2 \left(\frac{p_{t,j}d}{p_{t,\infty}L}\right)^b \tag{5}$$

$$C_{N,A} = K_3 \left(\frac{p_{t,j}d}{p_{t,\infty}L}\right)^c \tag{6}$$

where

$$a \approx b \approx 0.6$$

$$c \approx 0.7$$

For the present test condition,

$$\frac{h}{L} = K_1' \dot{m}^a = K_1'' J^a \tag{7}$$

$$\frac{l}{L} = K_2' \dot{m}^b = K_2'' J^b \tag{8}$$

$$C_{N,A} = K_3' \dot{m}^c = K_3'' J^c \tag{9}$$

where ' indicates mass flow and " indicates momentum. Equation (6) agrees quali-
tatively with the experimental results of reference 6.

It has been noted previously that the ratio of normal aerodynamic interaction force
to jet reaction force decreases as the jet throat width increases (refs. 4 and 16) and as
the ratio of jet total pressure to free-stream total pressure increases (refs. 2, 5, 8,
and 16). These trends are shown for the present data in figure 21(a) where the aerody-
namic to jet force ratios in coefficient form are plotted against $p_{t,j}/p_{t,\infty}$. The data on
this figure are grouped by nominal jet throat width. This decrease in force ratio can be
partially understood by comparing figure 19 with figure 21(a). Because $C_{N,R}$ increases
more rapidly with increasing jet mass flow (or jet momentum) than $C_{N,A}$ the ratio of
$C_{N,A}/C_{N,R}$ decreases as mass flow increases, as shown in figure 21(b). The increase
in jet mass flow or momentum was caused by increasing the jet total pressure and/or
increasing the jet throat width thereby causing $C_{N,A}/C_{N,R}$ to decrease as jet total
pressure and throat width increase.

The exact cause for the spread of the data for the 0.007-in. (0.0178 cm) throat
width in figures 21(a) and (b) is unknown; however, any inaccuracy in the throat width
calibration would have the greatest effect with the smallest throat width.

Included in figure 21(b) is a fairing of some unpublished data of secondary injection
from a slot near the base of a 9° half-angle cone. The trends shown for this three-
dimensional configuration are the same as those observed for the two-dimensional model
reported herein. However, the actual values of $C_{N,A}/C_{N,R}$ are less for the three-
dimensional cone than for the two-dimensional flat plate, as might be expected by the
results of reference 16.

The values of $F_{N,A}/F_{N,R}$ given in reference 4 are believed to be somewhat in
error due to the deflection of the plate forming the jet slot. The width of the slot was
not measured under pressurized conditions. The percentage of error increased in all
probability as the jet pressure was increased and as the nominal slot width was
decreased. However, the conclusion reached in reference 4 that the force ratio
$F_{N,A}/F_{N,R}$ increases with decreasing jet throat width at a given total pressure ratio
remains in agreement with the results presented herein.

The method employed to determine the aerodynamic interaction forces assumed the
absence of any three-dimensional-flow effects. However, three-dimensional effects do
exist near the edges of the jet, as shown by reference 16. In order to investigate the pos-
sibility that these three-dimensional effects were penetrating to the center line of the
plate and affecting the measured surface pressures (and consequently the aerodynamic
interaction forces), several runs were made with side plates on the model to make the
flow more nearly two dimensional. Jet throat widths varied from 0.005 in. (0.013 cm) to
0.054 in. (0.137 cm) and the jet total pressures were varied approximately through

12

the same range as for the other tests. The results of the tests with side plates are shown in figure 22, along with a solid line indicating faired values for the tests without side plates. The three-dimensional effects had a relatively small influence on the aerodynamic interaction force coefficients. The extra amount of aerodynamic interaction force due to the slightly longer separation distance and slightly higher pressures of the side plate case as opposed to the case without side plates as noted in figure 8 was not sufficient to produce a sizable increase in the value of $C_{N,A}$.

Supersonic jets.- Values of $C_{N,A}$ for jets of various exit Mach numbers and a jet throat width of approximately 0.020 in. (0.051 cm) are shown plotted against the jet mass flow parameter $\left(p_{t,j}/p_{t,\infty}\right)(d/L)$ in figure 23(a), and for a jet throat width of 0.010 in. (0.025 cm) in figure 23(b). Also shown are solid lines indicating the jet reaction force coefficients $C_{N,R}$ for the various jet Mach numbers. From these figures it is apparent that, for a given jet mass flow, the aerodynamic interaction force decreases and the jet reaction force increases as the jet exit Mach number increases. The decrease in $C_{N,A}$ as M_j increases is also indicated by the surface pressure distribution plots of supersonic jets in figure 13. For a nominally constant jet mass flow, as the jet exit Mach number increases the length of the separation region decreases.

A comparison of the data for the Mach 3.2 jets in figures 23(a) and (b) shows that the jet mass flow parameter $\left(p_{t,j}/p_{t,\infty}\right)(d/L)$ correlates values of $C_{N,A}$ reasonably well for different jet throat widths for the supersonic jets, as well as for the sonic jets.

In figures 24(a) and (b), values of the total normal force $C_{N,A} + C_{N,R}$ are plotted against $\left(p_{t,j}/p_{t,\infty}\right)(d/L)$ for jet throat widths of approximately 0.020 in. (0.051 cm) and 0.010 in. (0.025 cm), respectively. Also in these figures are solid lines indicating values of $C_{N,R}$ for the various jet Mach numbers. These two figures show that, although at a given jet mass flow $C_{N,A}$ decreases and $C_{N,R}$ increases as M_j increases, the sum of $C_{N,A}$ and $C_{N,R}$ remains nominally a constant for a given jet mass flow regardless of the jet exit Mach number. Therefore, under the conditions of this test program, a given jet mass flow produces a given total amount of force, regardless of how this force is divided into the reaction and aerodynamic interaction components.

The data of figures 23 and 24 are replotted in figures 25 and 26, respectively, with the jet momentum parameter (eq. (3)) used to correlate the data, instead of the mass flow parameter (eq. (1)). With varying values of M_j, jet mass flow and jet momentum are not directly proportional to each other, and the effect of momentum can be examined. The jet momentum parameter offers no apparent advantage over the mass flow parameter in correlating $C_{N,A}$ and is not nearly as good as mass flow for correlating $C_{N,A} + C_{N,R}$.

Schlieren photographs of some of the supersonic jets are shown in figure 27. The shock structure from these photographs is not as clear for the supersonic as for the sonic jets. From this figure it is apparent that the general appearance of a supersonic jet is

similar to that of a sonic jet, although the supersonic jet does not expand as much for a • given value of $\left(p_{t,j}/p_{t,\infty}\right)$ as does the sonic jet (ref. 11). The amount of this expansion decreases as the jet Mach number increases due to the decrease of static pressure at the jet exit with the increase of Mach number. The Mach 6.2 jet nozzle configuration was not fully started unless the value of $\left(p_{t,j}/p_{t,\infty}\right)(d/L)$ was above approximately 0.00055.

CONCLUDING REMARKS

The effects of two-dimensional secondary jets issuing approximately perpendicular to a flat plate have been investigated at a free-stream Mach number of 6. The parameters varied were secondary jet exit Mach number (1 to 6), jet total pressure, and jet orifice width. Free-stream tunnel conditions and secondary jet total temperatures remained constant. The boundary layer on the plate in the vicinity of the jet was turbulent. In addition to jet shock structures, jet penetrations, and separation distances, the gross aerodynamic forces as determined from surface pressure distributions were examined. The magnitude of the surface pressures ahead of the jet exit position can be largely determined from boundary-layer separation considerations. However, the extent of the separation region is determined by the jet penetration height, an indication of which was obtained from measurements of the jet strong-shock standoff distance from the plate surface. The separation distances, jet strong-shock standoff distances, and aerodynamic normal forces for the sonic jet with various slot widths can be correlated with the use of a parameter which for this investigation is proportional to the jet mass flow (and the jet momentum). The ratio of the aerodynamic normal-force coefficient to the reaction normal-force coefficient increases with decreasing jet mass flow (and jet momentum). Therefore, the force ratio will increase as either slot width or jet total pressure is decreased. However, the force ratio remains approximately constant for any given jet mass flow (or jet momentum) regardless of slot width or jet pressure ratio. For the sonic jets, the force ratio varied from approximately 1.7 to 0.8. The data for the conditions of this investigation show that the aerodynamic normal force for a given jet mass flow decreases with increasing jet exit Mach number but the total normal force (including reaction) is a constant for a given jet mass flow and independent of jet exit Mach number. The jet momentum parameter offers no apparent advantage over the mass flow parameter in correlating the aerodynamic force, and, when the jet exit Mach number varies, the mass flow parameter is a more effective correlating parameter for the total normal force.

Langley Research Center,
National Aeronautics and Space Administration,
Langley Station, Hampton, Va., August 8, 1966,
129-01-09-15-23.

REFERENCES

1. Morkovin, M. V.; Pierce, C. A.; and Craven, C. E.: Interaction of a Side Jet With a Supersonic Main Stream. Bull. No. 35, Eng. Res. Inst., Univ. of Michigan, Sept. 1952.

2. Vinson, P. W.; Amick, J. L.; and Liepman, H. P.: Interaction Effects Produced by Jet Exhausting Laterally Near Base of Ogive-Cylinder Model in Supersonic Main Stream. NASA MEMO 12-5-58W, 1959.

3. Ferrari, Carlo: Interference Between a Jet Issuing Laterally From a Body and the Enveloping Supersonic Stream. Bumblebee Rept. No. 286 (Contract NOrd 7386), Appl. Phys. Lab., Johns Hopkins Univ., Apr. 1959.

4. Romeo, David J.; and Sterrett, James R.: Aerodynamic Interaction Effects Ahead of a Sonic Jet Exhausting Perpendicularly From a Flat Plate Into a Mach Number 6 Free Stream. NASA TN D-743, 1961.

5. Broadwell, James E.: Correlation of Rocket Nozzle Gas Injection Data. AIAA J. (Tech. Notes Comments), vol. 1, no. 8, Aug. 1963, pp. 1911-1913.

6. Strike, W. T.; Schueler, C. J.; and Deitering, J. S.: Interactions Produced by Sonic Lateral Jets Located on Surfaces in a Supersonic Stream. AEDC-TDR-63-22, U.S. Air Force, Apr. 1963.

7. Charwat, A. F.; and Allegre, J.: Interaction of a Supersonic Stream and a Transverse Supersonic Jet. AIAA J., vol. 2, no. 11, Nov. 1964, pp. 1965-1972.

8. McDonald, R. D.; Vinson, P. W.; and Mayes, J. F.: A Study of Three Hypersonic Missile Control Devices. Res. Rept. OR 3978, Martin Co., June 1964.

9. Mitchell, John W.: An Analytical Study of a Two-Dimensional Flow Field Associated With Sonic Secondary Injection Into a Supersonic Stream. Vidya Tech. Note 9166-TN-2 (Contract AF 04(611)-9075), Itek Corp., Mar. 1964.

10. Kaufman, Louis G., II.: Classification of Interactions Due to High-Speed Flows Past Transverse Jets. Res. Rept. RE-154, Grumman Aircraft Eng. Corp., Feb. 1962.

11. Sterrett, James R.; and Barber, John B.: A Theoretical and Experimental Investigation of Secondary Jets in a Mach 6 Free Stream With Emphasis on the Structure of the Jet and Separation Ahead of the Jet. Presented at the Separated Flows Specialists Meeting, Fluid Dynamics Panel (Brussels, Belgium), AGARD, May 9-11, 1966.

12. Sterrett, James R.; and Emery, James C.: Extension of Boundary-Layer-Separation Criteria to a Mach Number of 6.5 by Utilizing Flat Plates With Forward-Facing Steps. NASA TN D-618, 1960.

13. Holloway, Paul F.; and Sterrett, James R.: Effect of Controlled Surface Roughness on Boundary-Layer Transition and Heat Transfer at Mach Numbers of 4.8 and 6.0. NASA TN D-2054, 1964.

14. Korst, H. H.: Dynamics and Thermodynamics of Separated Flows. Single and Multi-Component Flow Processes, R. L. Peskin and C. F. Chen, eds., Eng. Res. Publ. No. 45, Rutgers — The State Univ., 1965, pp. 69-107.

15. Chapman, Dean R.; Kuehm, Donald M.; and Larson, Howard K.: Investigation of Separated Flows in Supersonic and Subsonic Streams With Emphasis on the Effect of Transition. NACA Rept. 1356, 1958. (Supersedes NACA TN 3869.)

16. Romeo, David J.: Aerodynamic Interaction Effects Ahead of Rectangular Sonic Jets Exhausting Perpendicularly From a Flat Plate Into a Mach Number 6 Free Stream. NASA TN D-1800, 1963.

Flow
→

Boundary-layer trips

Jet location

Removable backpiece

Nozzle piece

10°

19.25-inch (48.9 cm) long plate
1.00-inch (2.54 cm) thick

Airflow
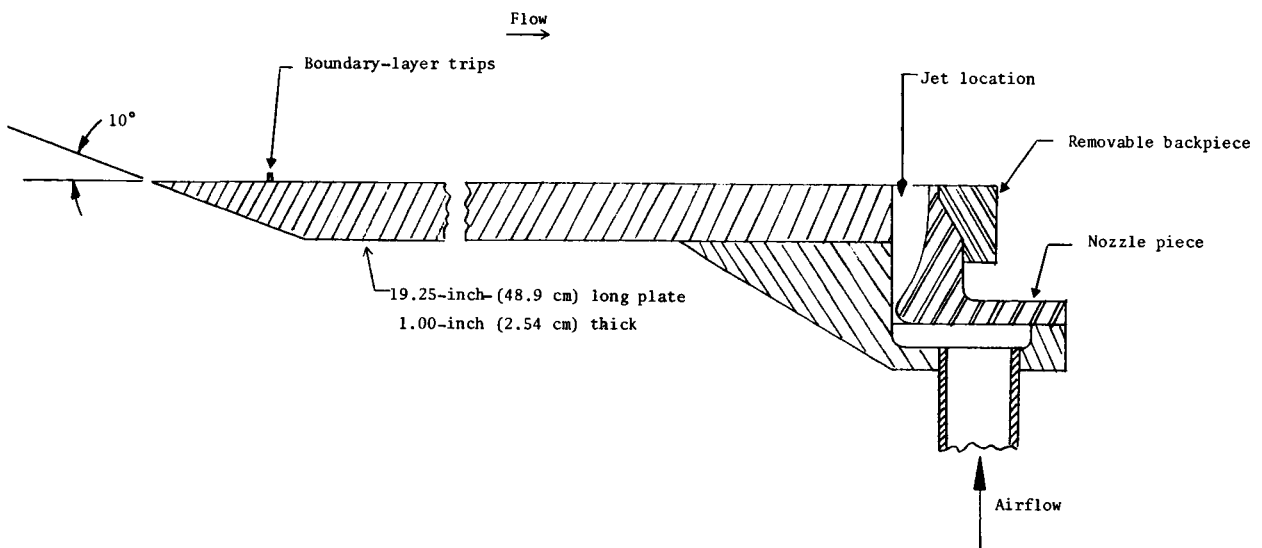
(a) Sectional view of plate.
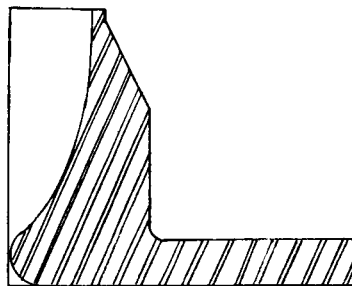
(b) Mach 6.2 nozzle.
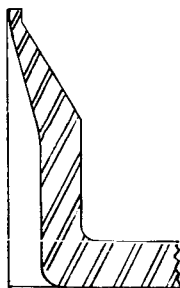
(c) Sonic nozzle.
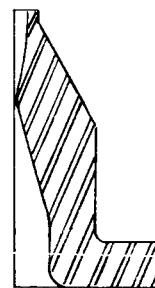
(d) Typical supersonic nozzle.

Figure 1.- Flat plate configuration.
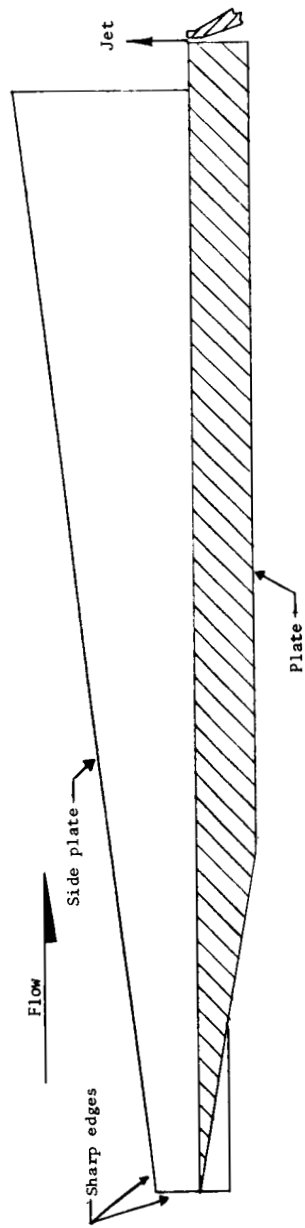
(e) Side plate configuration.
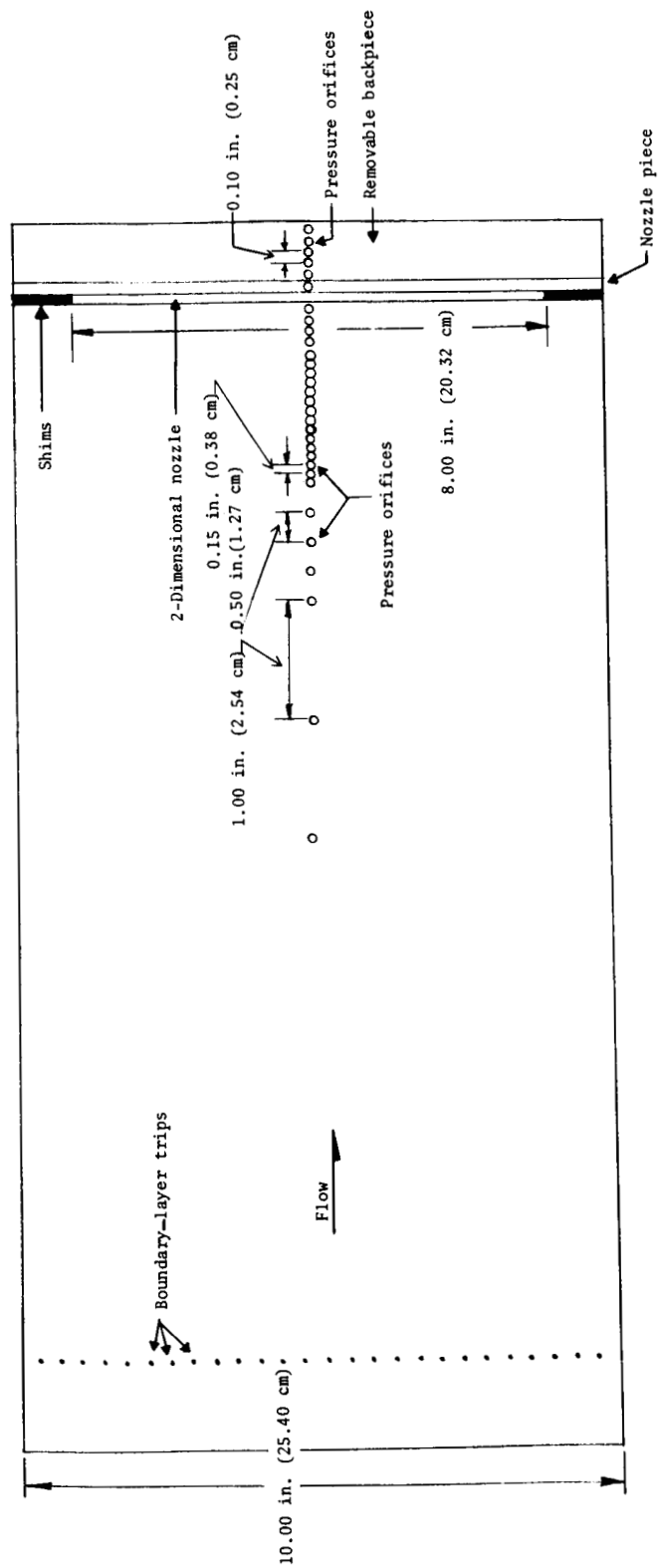
(f) Plan of top surface of model plate.

Figure 1.- Concluded.
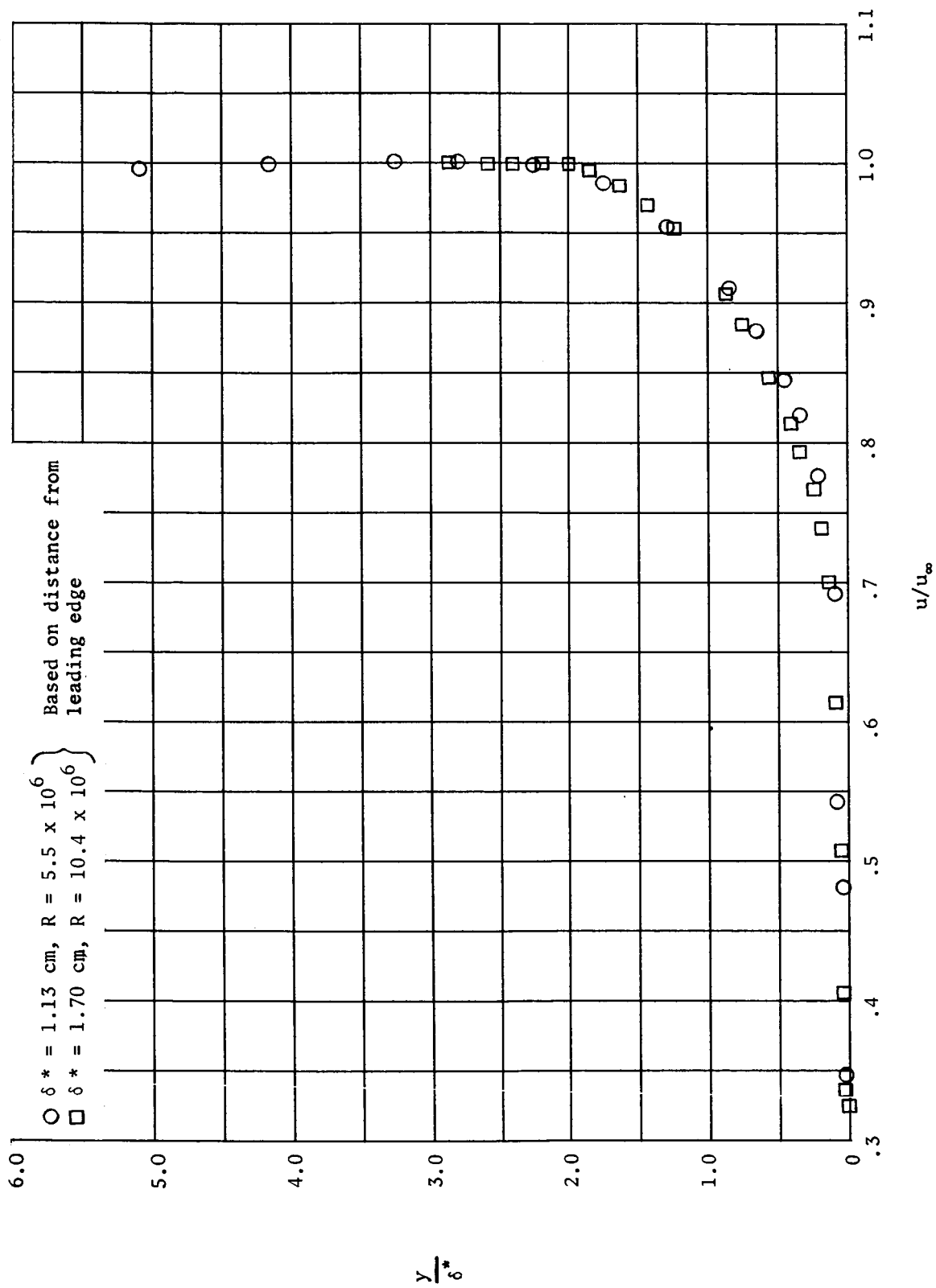
Figure 2.- Boundary-layer velocity profiles on plate with roughness; $R_\infty = 8.1 \times 10^6$ per ft $(26.5 \times 10^6 \text{ per m})$; $\frac{T_W}{T_{t,\infty}} = 0.89$.

Expansions

Internal shock

Side boundary

Side boundary

Region A

Region B

Internal shock

1   2

(a) Characteristic layout.

Strong shock   Subsonic

Region C

Reflected shock

Expansions

Supersonic

Slipline

Supersonic inner core

Internal shock

Side boundary

Region A

Region B
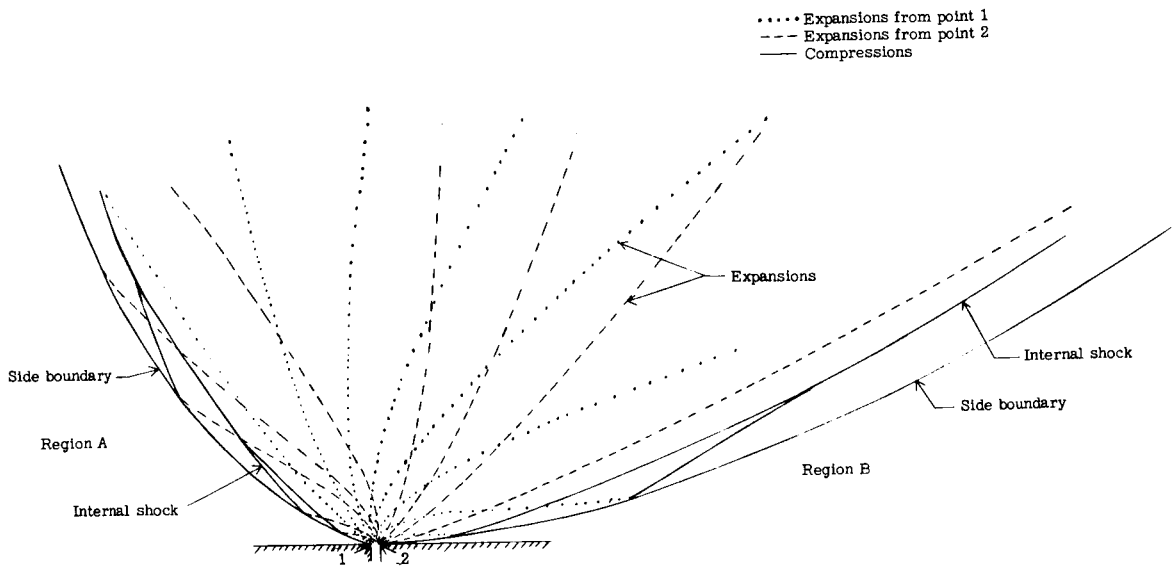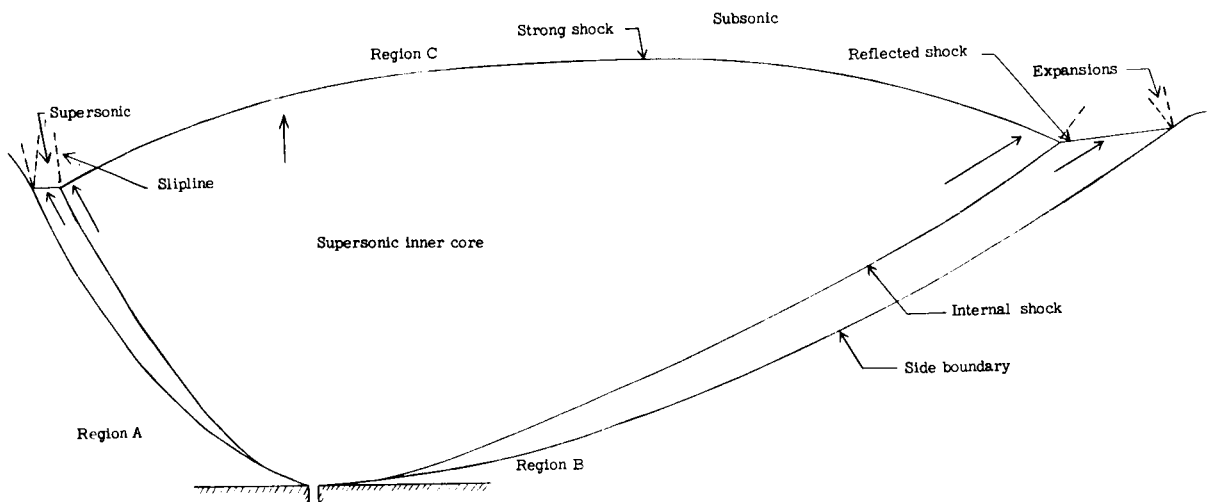
(b) Sketch of actual jet structure.

Figure 3.- Schematic flow diagram for free jet. $\dfrac{p_A}{p_{t,j}} = 0.00524$; $\dfrac{p_B}{p_{t,j}} = 0.000629$.
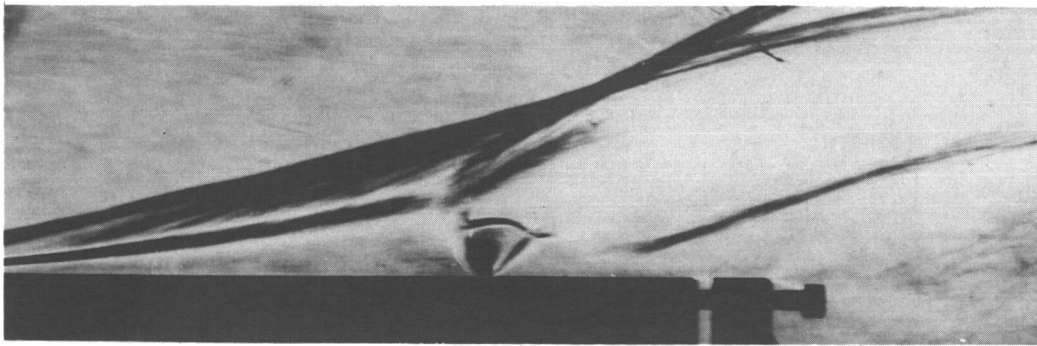
(a) Reproduction of figure 14 from reference 4.
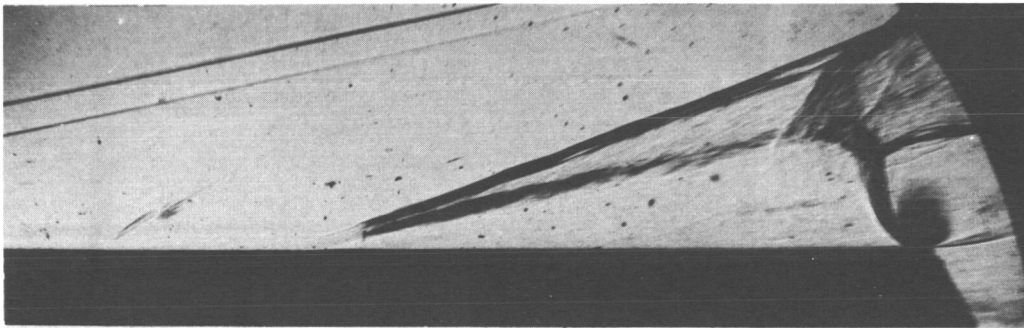
(b) Schlieren photograph; $M_j = 1.0$; $\dfrac{p_{t,j}}{p_{t,\infty}} = 0.76$.

—·—· Jet strong shock

———— Internal shock

······ Reflected shock
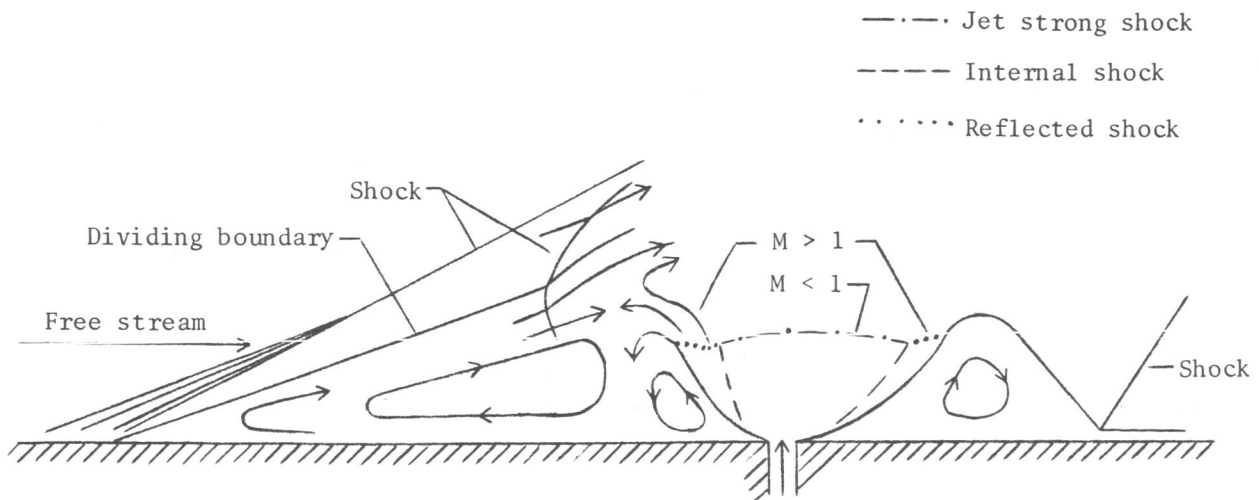
(c) Schematic of flow.

Figure 4.- Examples of flow fields with underexpanded jets. $M_\infty = 6.0$.

L-66-7601

Disturbance associated with roughness elements

Reference bar outside of tunnel

Leading-edge shock

(a) Schlieren photograph.

$$\frac{p}{p_{t,\infty}}$$

Third peak pressure

Second peak pressure

First peak pressure

$$\frac{p_{\infty}}{p_{t,\infty}}$$

Jet

x, in.

x, cm
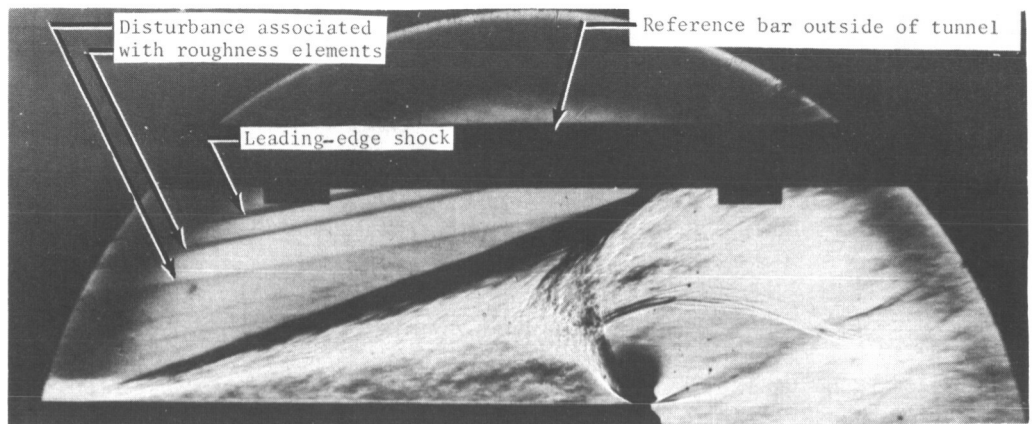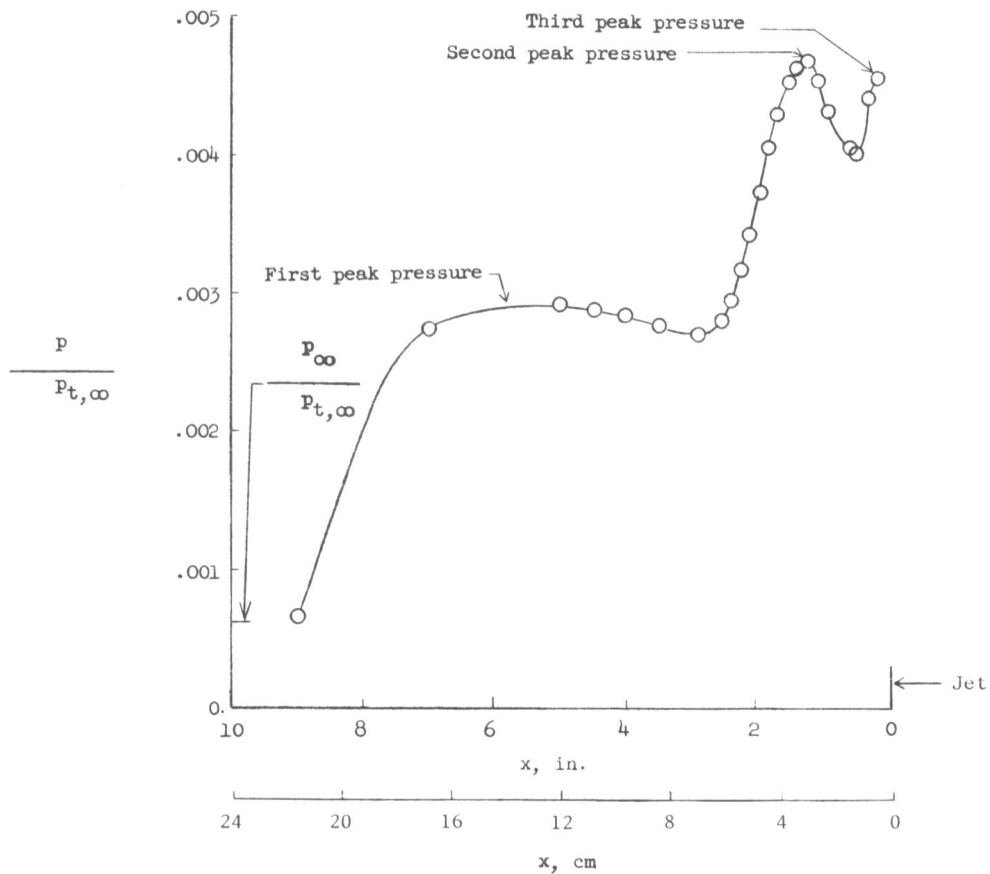
(b) Pressure distribution.

L-66-7602

Figure 5.- Pressure distribution and schlieren photograph illustrating the relationship between flow patterns and pressure regions. $M_j = 1.0$; $d = 0.054$ in. $(0.137$ cm$)$; $\frac{p_{t,j}}{p_{t,\infty}} = 0.34$.

22
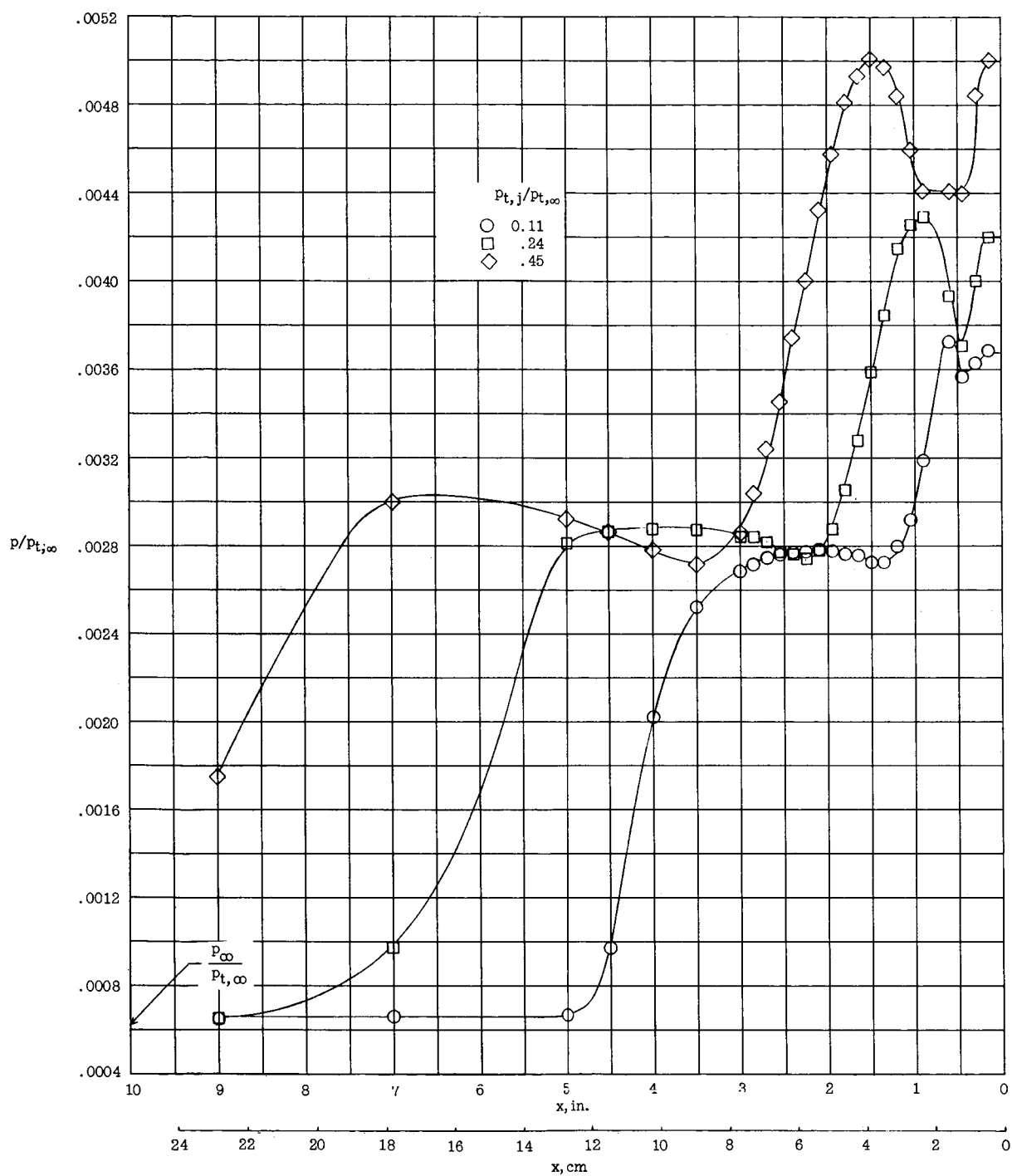
(a) d ≈ 0.054 in. (0.137 cm).

Figure 6.- Chordwise pressure distributions ahead of a jet for varying pressure ratios and slot widths. M_j = 1.0.
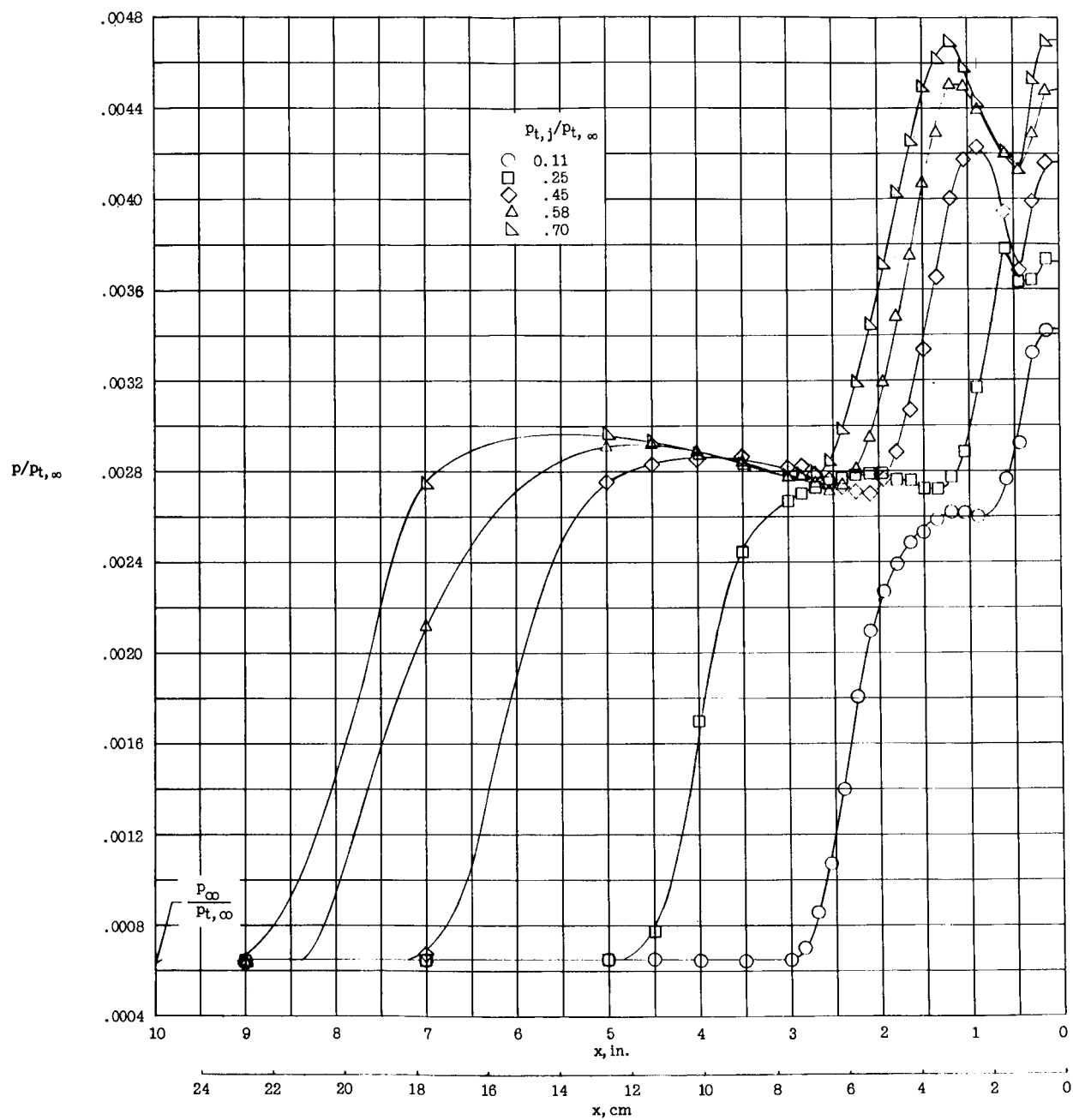
(b) $d \approx 0.024$ in. (0.061 cm).

Figure 6.- Continued.
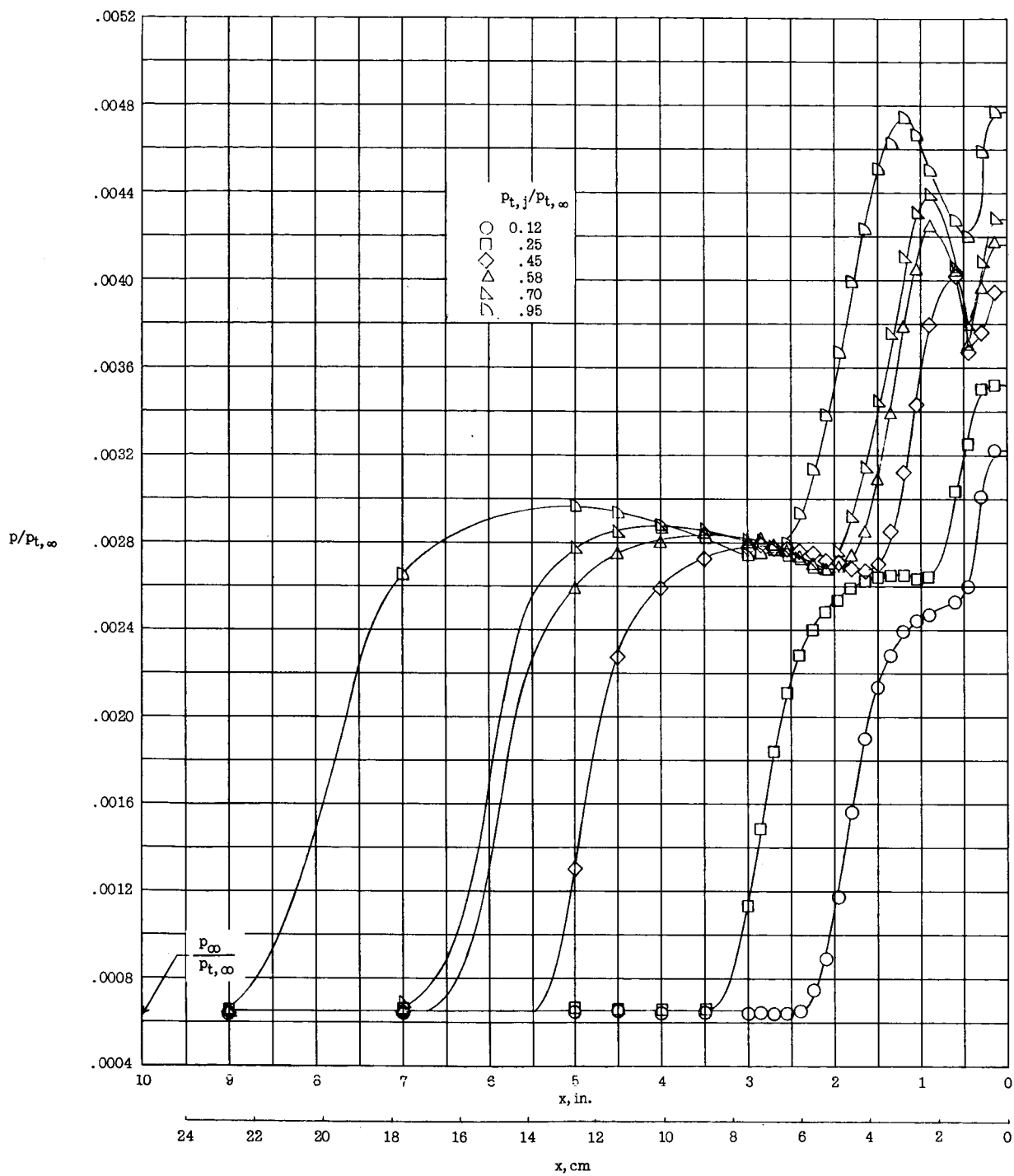
(c) d ≈ 0.015 in. (0.038 cm).

Figure 6.- Continued.
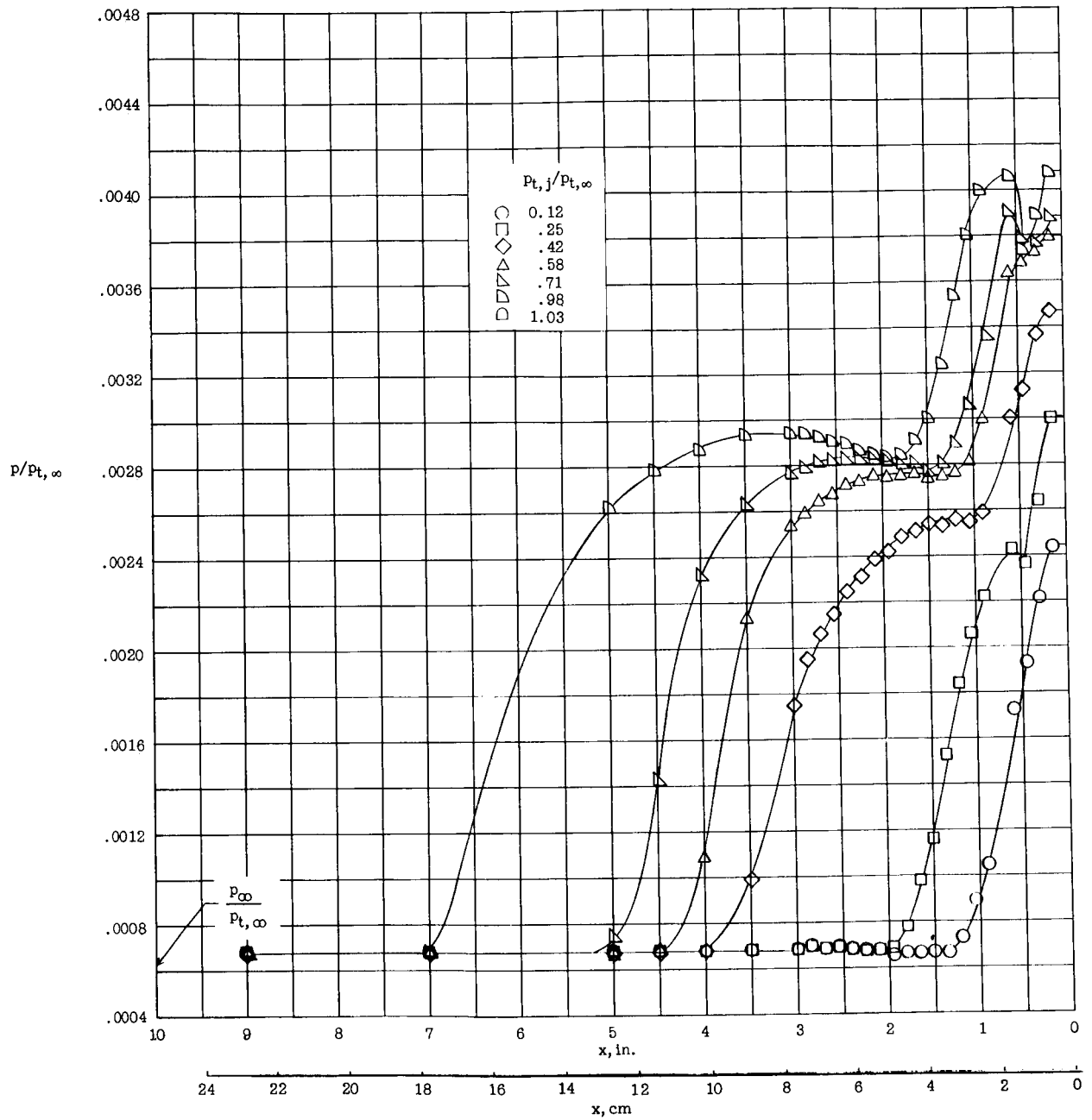
(d) d ≈ 0.007 in. (0.018 cm).

Figure 6.- Concluded.
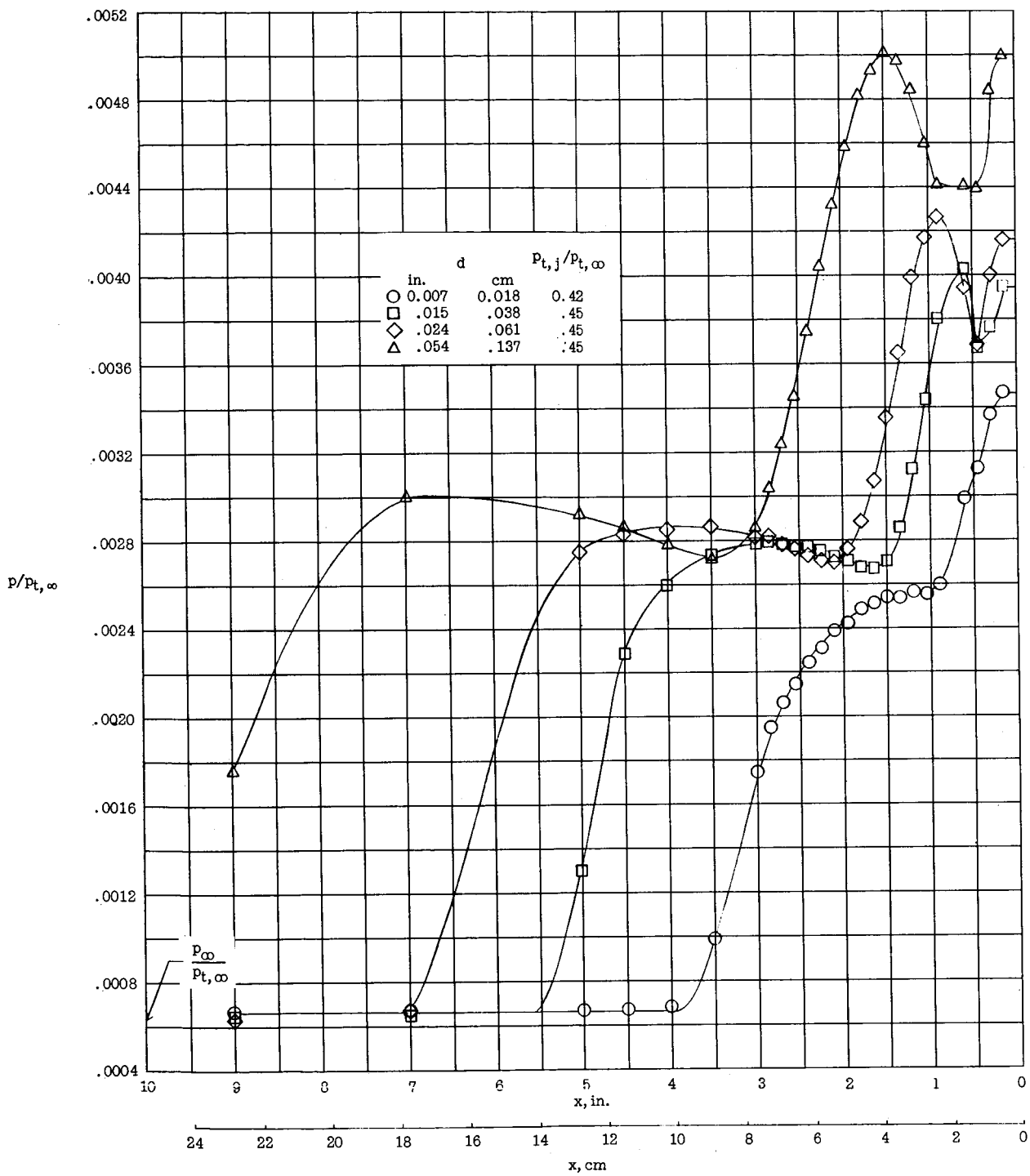
Figure 7.- Comparison of chordwise pressure distribution for various slot widths at nominally equal pressure ratio $\left(\dfrac{p_{t,j}}{p_{t,\infty}} \approx 0.45\right)$.
$M_j = 1.0$.
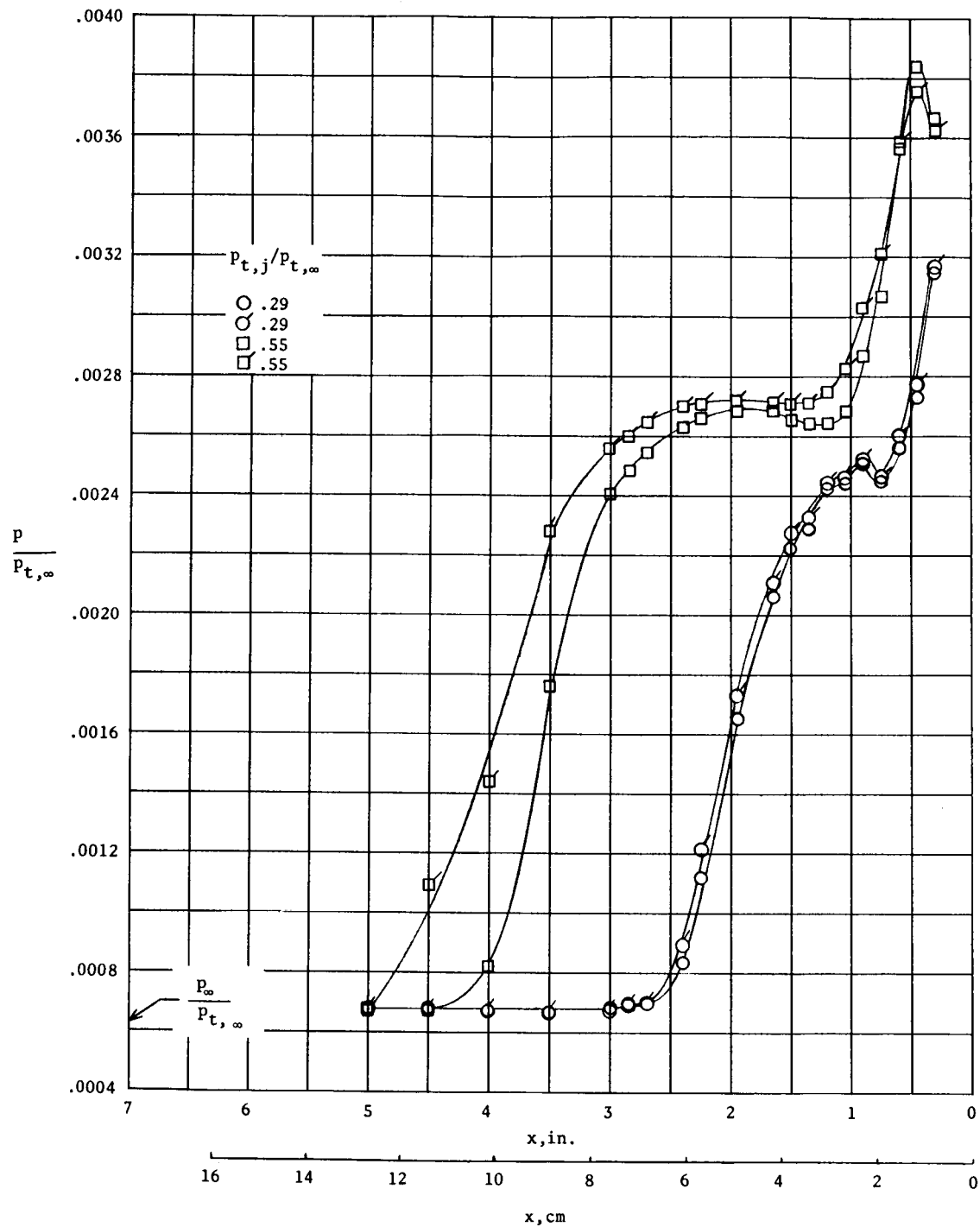
Figure 8.- Effect of side plates on surface pressure distributions. $M_j = 1.0$; $d \approx 0.005$ in. (0.013 cm). Symbols with ticks are for model with side plates.

28
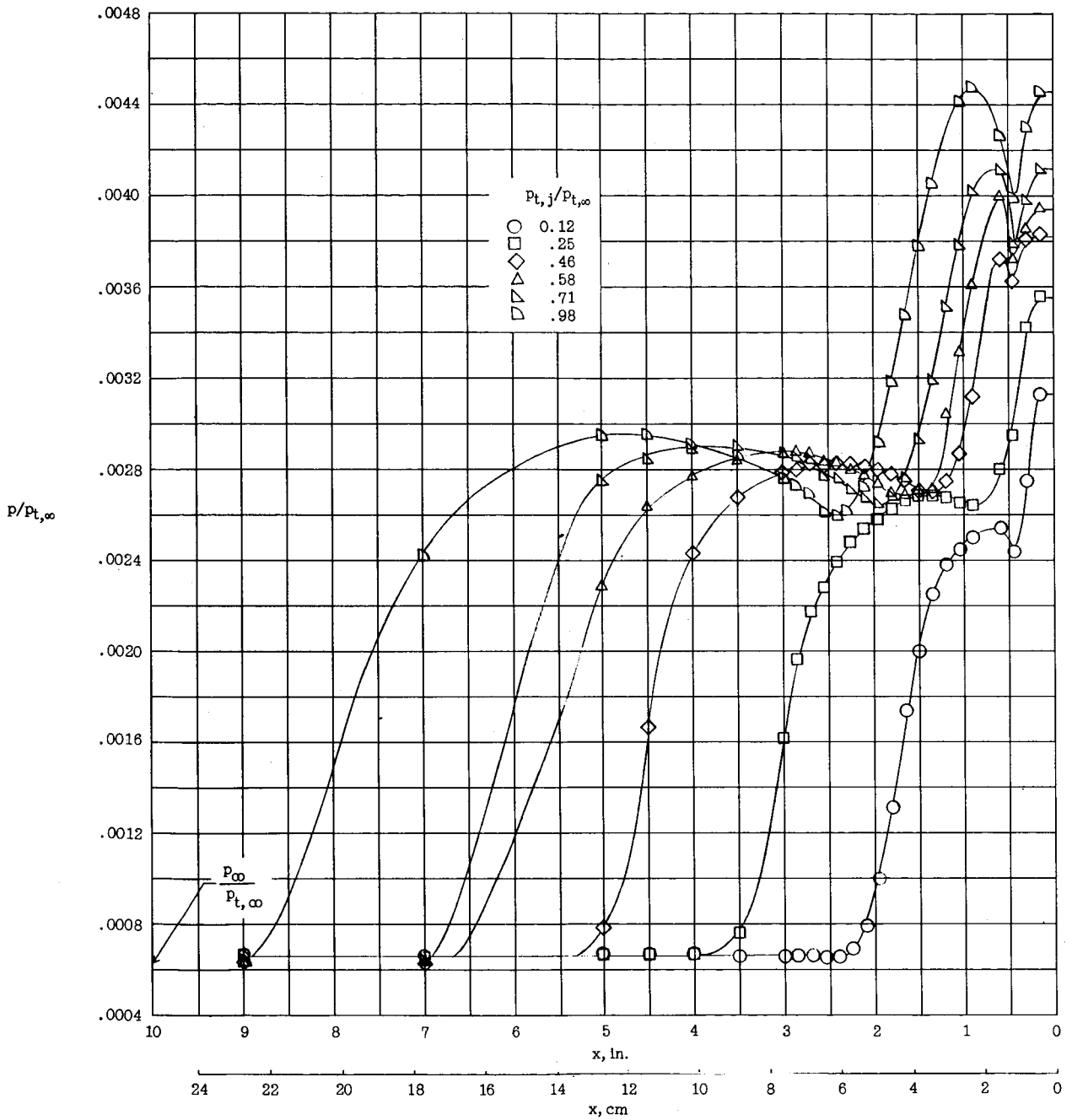
Figure 9.- Chordwise pressure distribution ahead of a jet for varying jet pressure ratio. M_j = 2.0; d ≈ 0.020 in. (0.051 cm).

$p/p_{t,\infty}$

.0048
.0044
.0040
.0036
.0032
.0028
.0024
.0020
.0016
.0012
.0008
.0004

$p_{t,j}/p_{t,\infty}$

○ 0.12
□ .25
◇ .46
△ .58
◁ .71
▷ .98

$\dfrac{p_{\infty}}{p_{t,\infty}}$

x, in.
10   9   8   7   6   5   4   3   2   1   0

x, cm
24   22   20   18   16   14   12   10   8   6   4   2   0
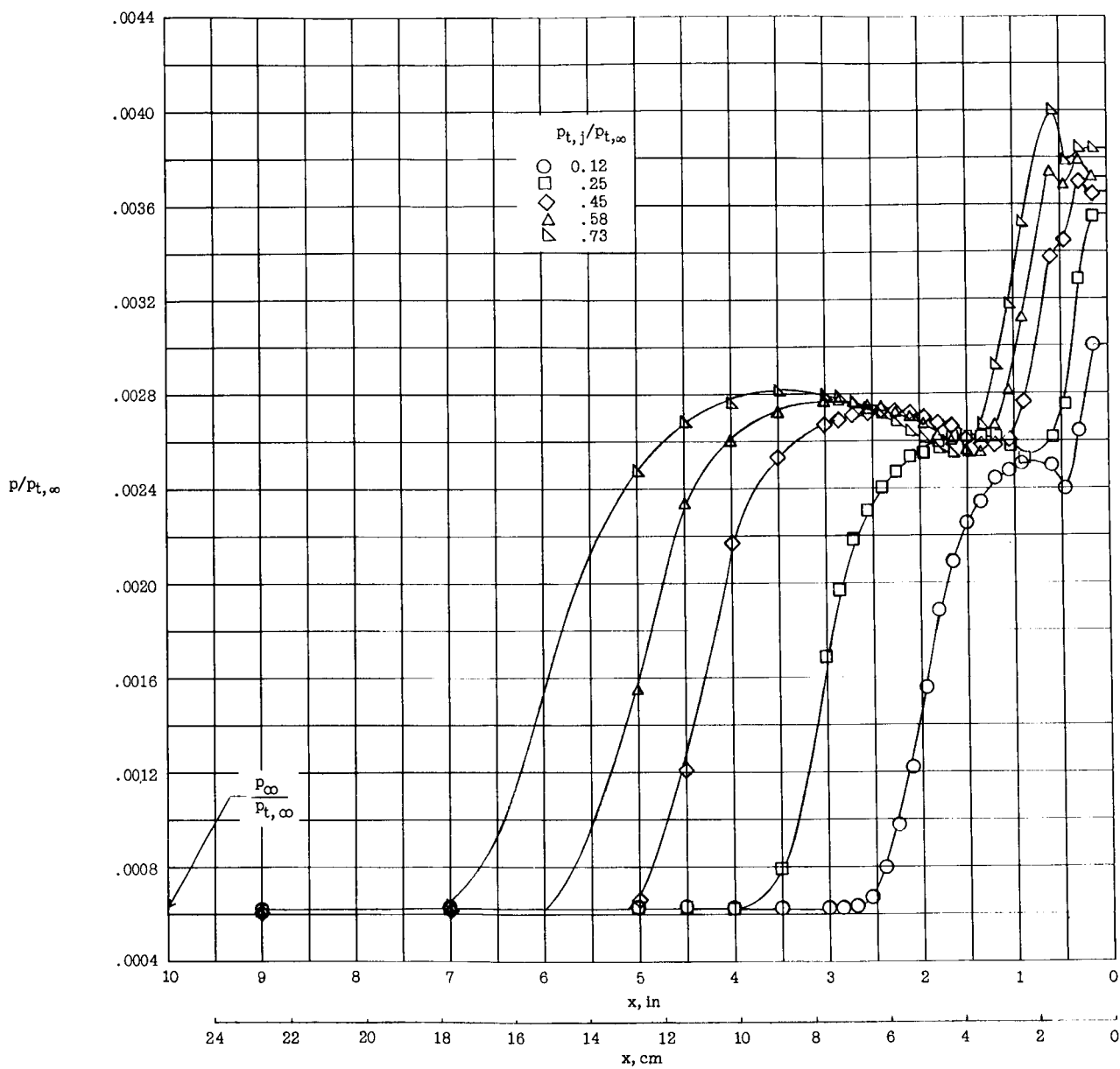
(a) $d \approx 0.020$ in. (0.051 cm).

Figure 10.- Chordwise pressure distribution ahead of a jet for varying pressure ratio. $M_j = 3.2$.
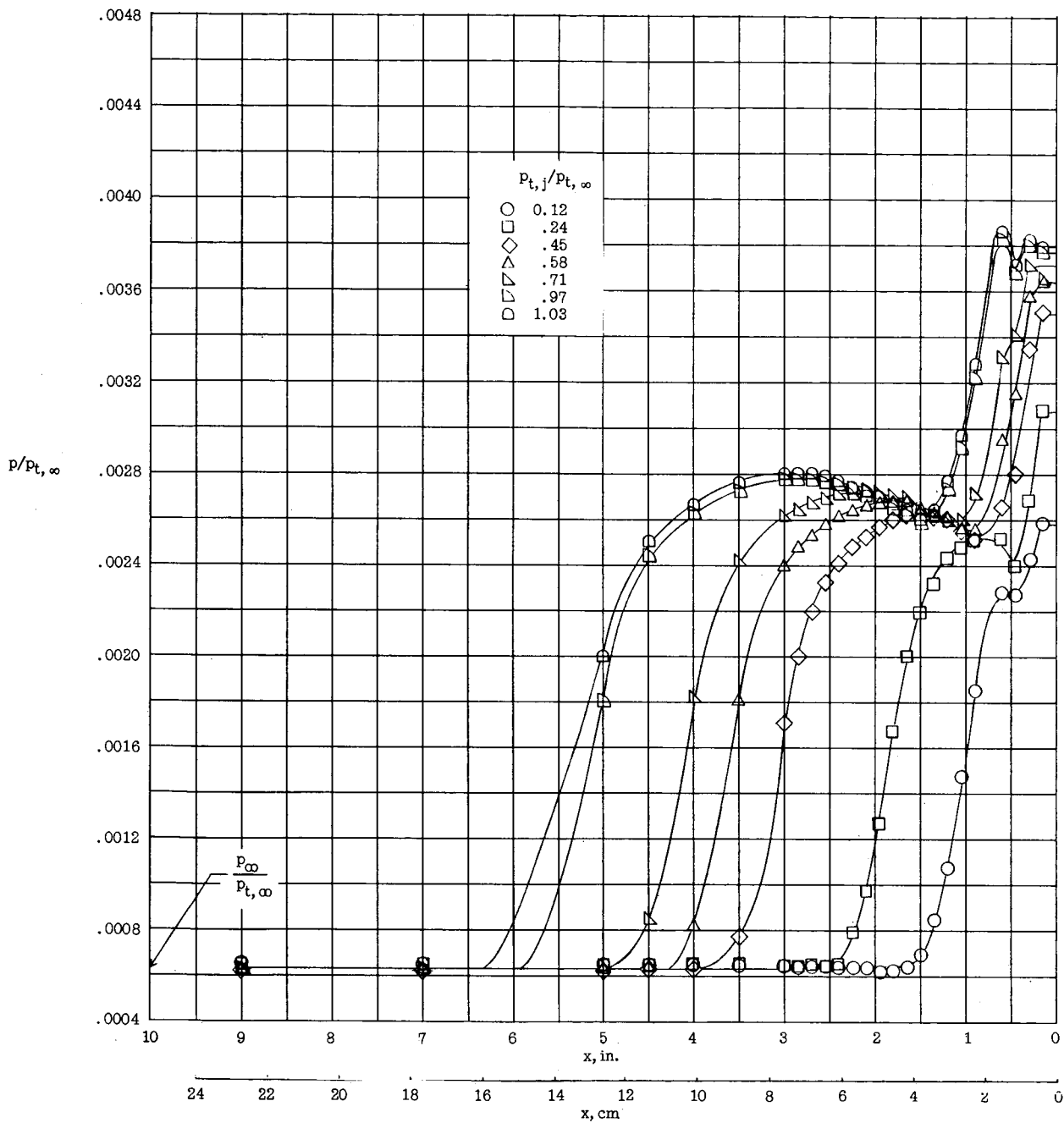
(b) $d \approx 0.010$ in. (0.025 cm).

Figure 10.- Concluded.
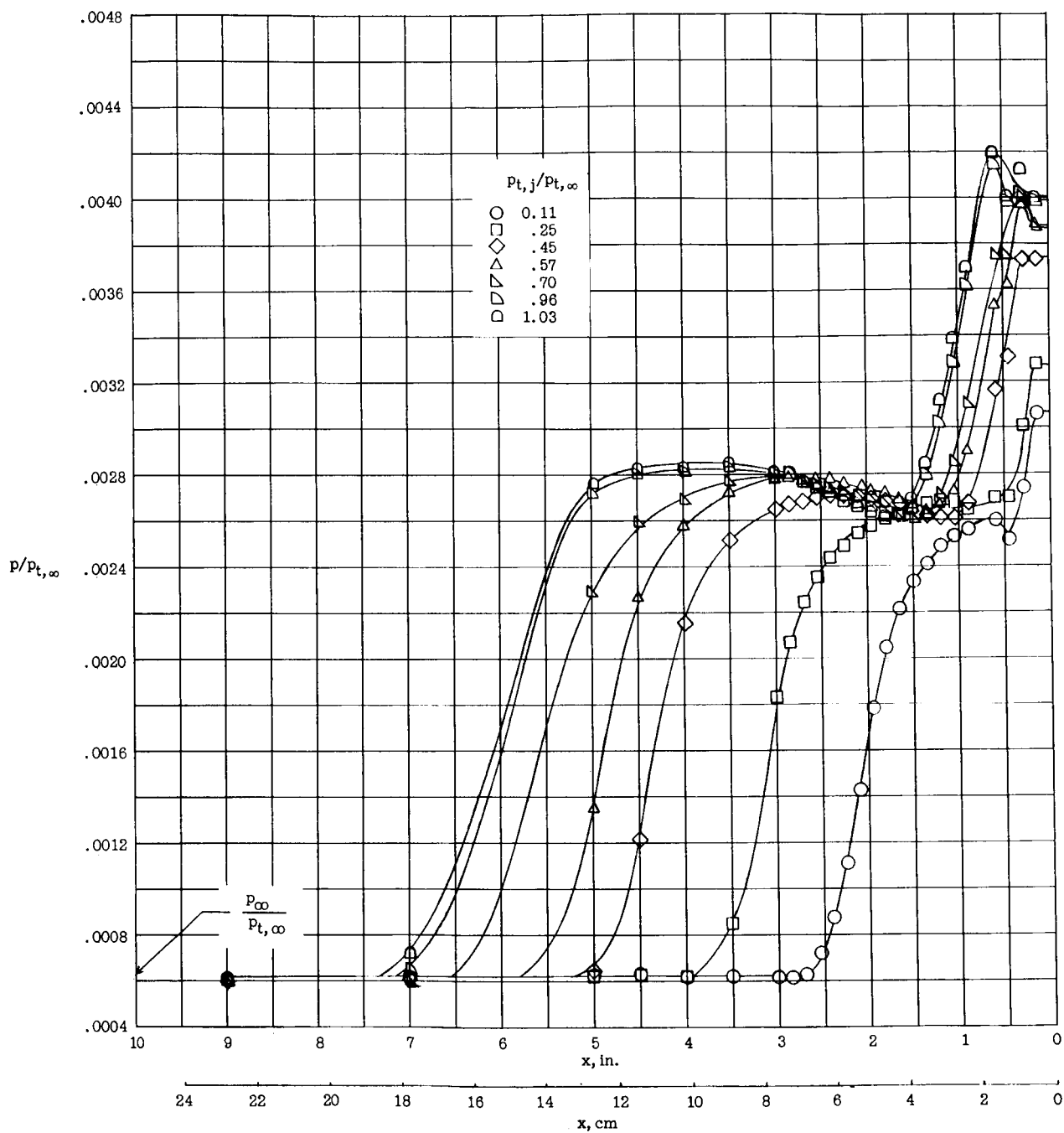
Figure 11.- Chordwise pressure distribution ahead of a jet for varying jet pressure ratio. M_j = 4.0; d ≈ 0.020 in. (0.051 cm).
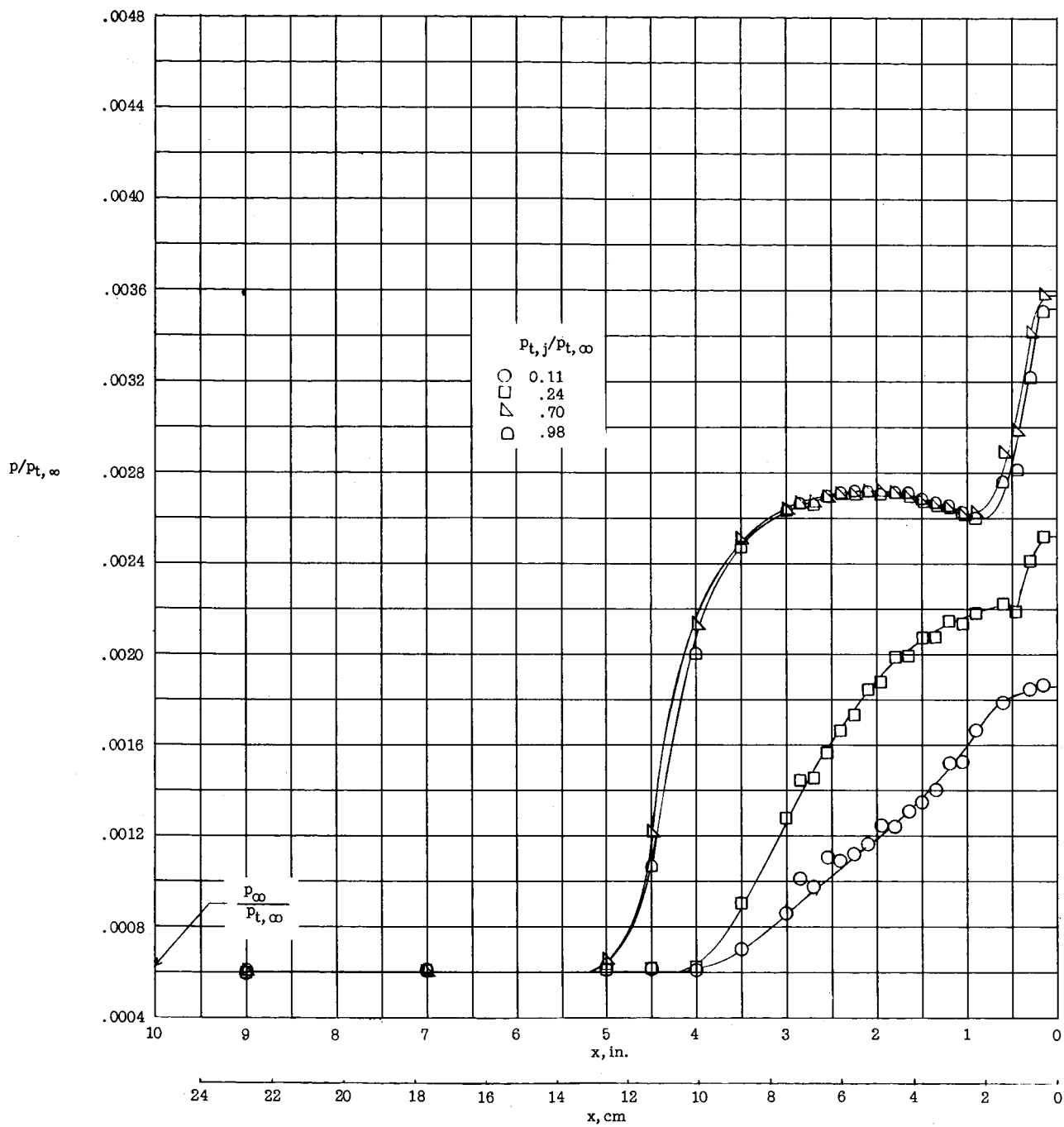
Figure 12.- Chordwise pressure distribution ahead of a jet with varying pressure ratio. $M_j = 6.2$; $d \approx 0.010$ in. (0.025 cm).
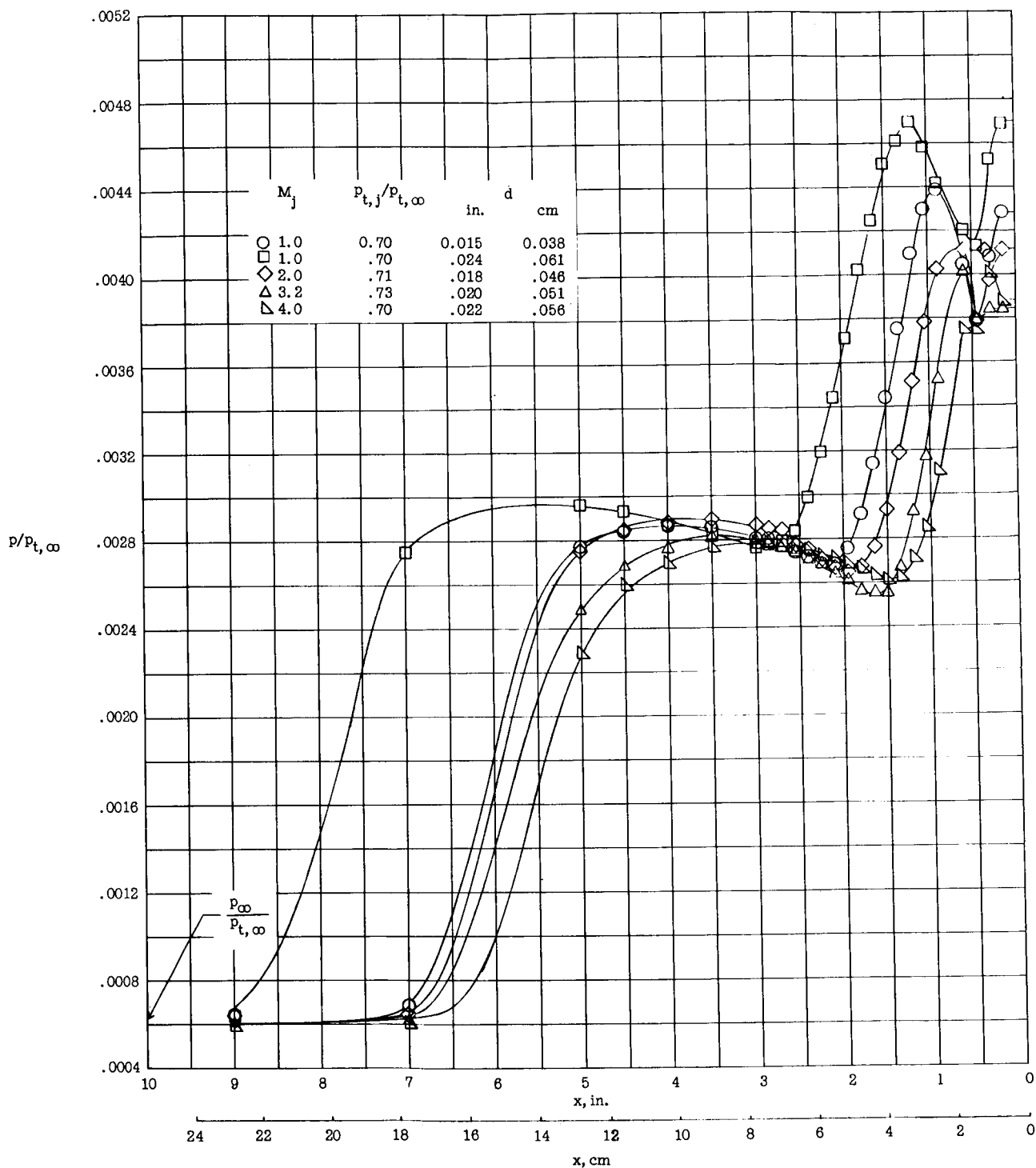
Figure 13.- Chordwise pressure distribution ahead of jet for various exit Mach number jets. $\frac{p_{t,j}}{p_{t,\infty}} \approx 0.70.$

$$\frac{p_{p1}}{p_{t,\infty}}$$

.004

.002

$$\frac{p_\infty}{p_{t,\infty}}$$

	in.	d	cm
○	0.007		0.018
□	.015		.038
◇	.024		.061
△	.054		.137

0   .0002   .0004   .0006   .0008   .0010   .0012   .0014

$$\left(p_{t,j}/p_{t,\infty}\right)\frac{d}{L}$$

(a) $M_j = 1.0$.

.004

— — First peak pressure for step from ref. 12 $\left(\dfrac{p_{p1} - p_o}{q_o} = 0.13 - \dfrac{1.5}{M_o^2} + \dfrac{9.1}{M_o^3}\right)$

$$\frac{p_{p1}}{p_{t,\infty}}$$

.002

$$\frac{p_\infty}{p_{t,\infty}}$$

	M_j	in.	d	cm
○	1.0	0.015		0.038
◇	3.2	.010		.025
△	6.2	.011		.028

0   .0002   .0004   .0006   .0008   .0010   .0012   .0014

$$\left(p_{t,j}/p_{t,\infty}\right)\frac{d}{L}$$

(b) $M_j \geqq 1.0$; $d \approx 0.010$ in. (0.025 cm).

.004

$$\frac{p_{p1}}{p_{t,\infty}}$$

.002

$$\frac{p_\infty}{p_{t,\infty}}$$

	M_j	in.	d	cm
○	1.0	0.024		0.061
□	2.0	.018		.046
◇	3.2	.020		.051
△	4.0	.022		.056

0   .0002   .0004   .0006   .0008   .0010   .0012   .0014

$$\left(p_{t,j}/p_{t,\infty}\right)\frac{d}{L}$$
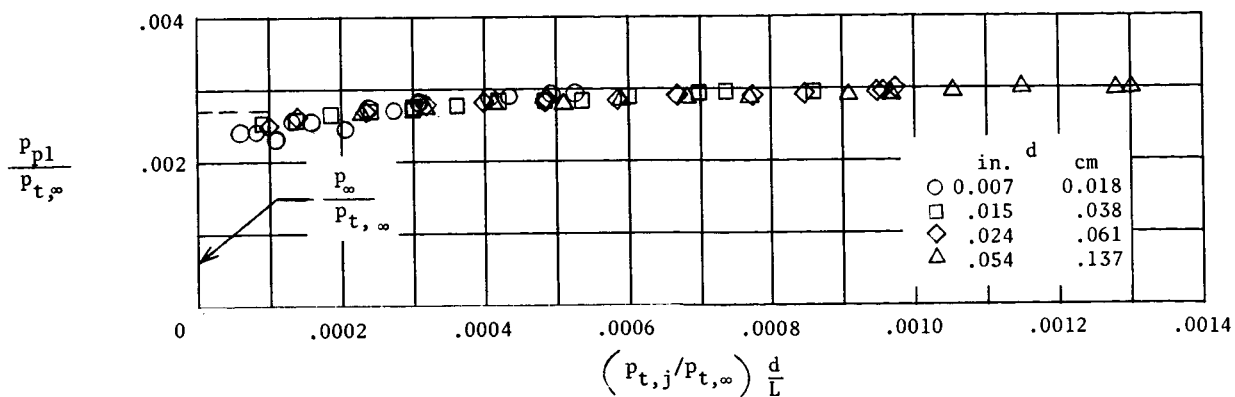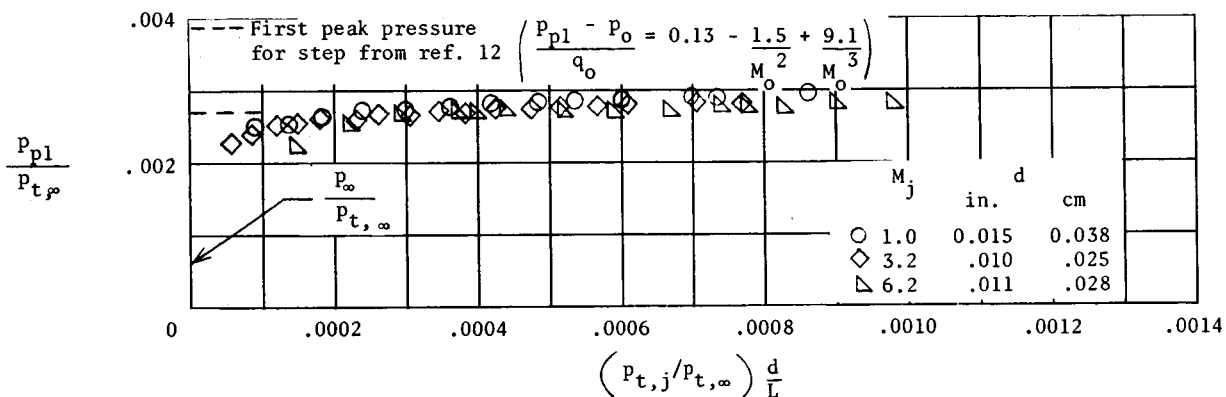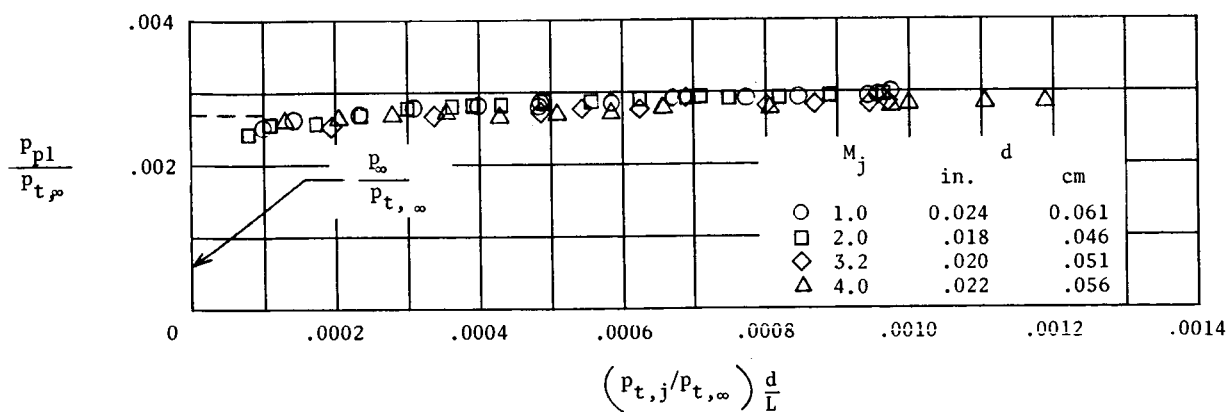
(c) $M_j \geqq 1.0$; $d \approx 0.020$ in. (0.051 cm).

Figure 14.- First peak pressures.
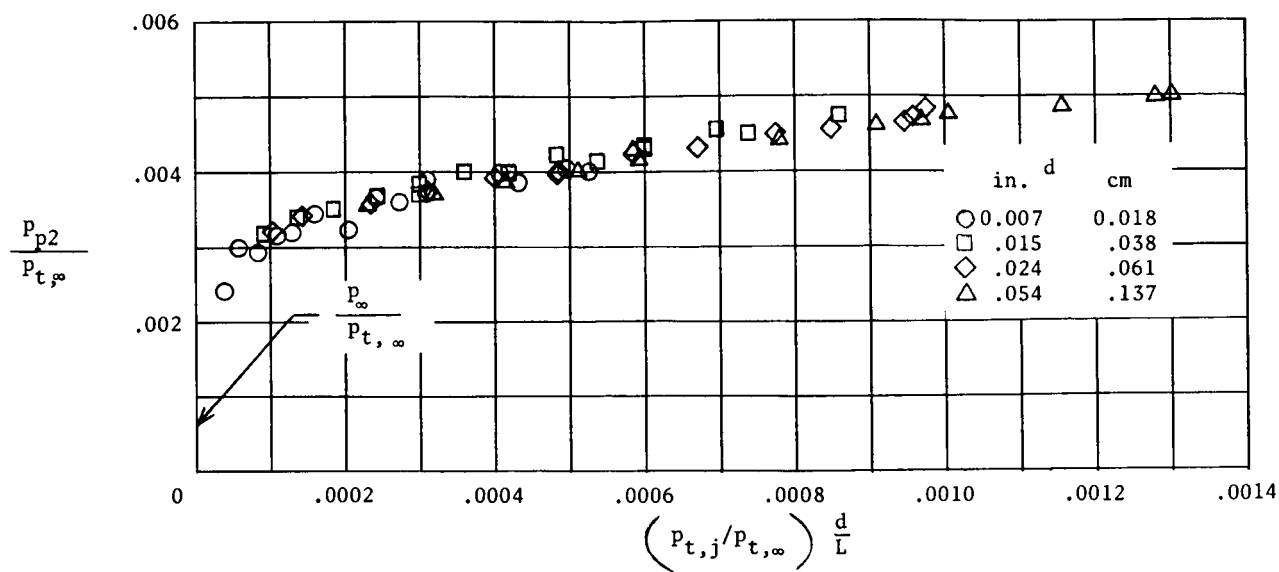
(a) $M_j = 1.0$.
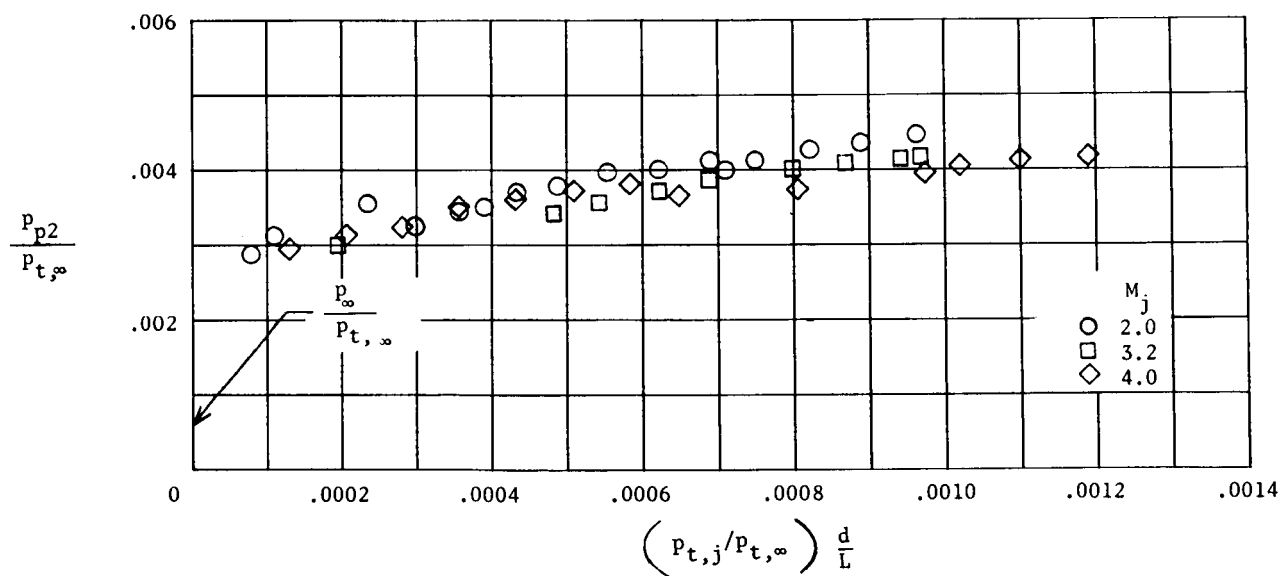
(b) $M_j > 1.0$; $d \approx 0.020$ in. (0.051 cm).

Figure 15.- Second peak pressures.
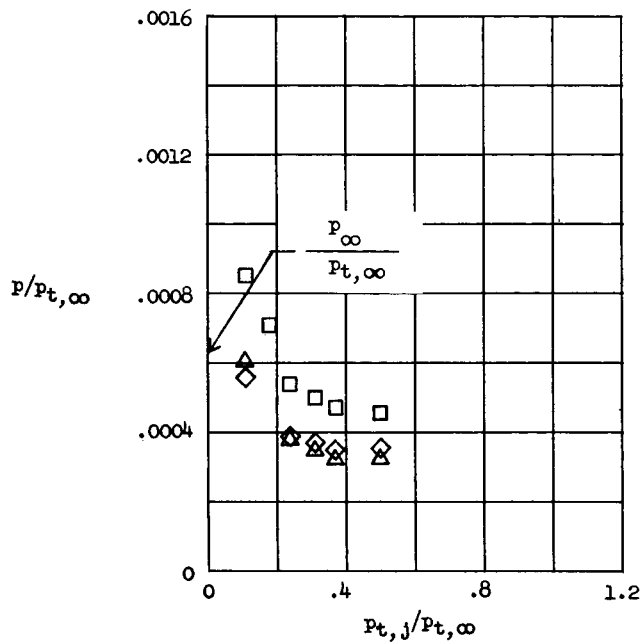
(a) d ≈ 0.05 in. (0.13 cm).
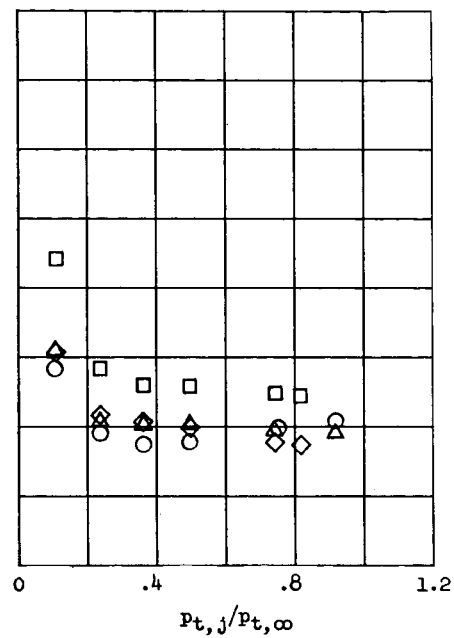
(b) d ≈ 0.02 in. (0.05 cm).
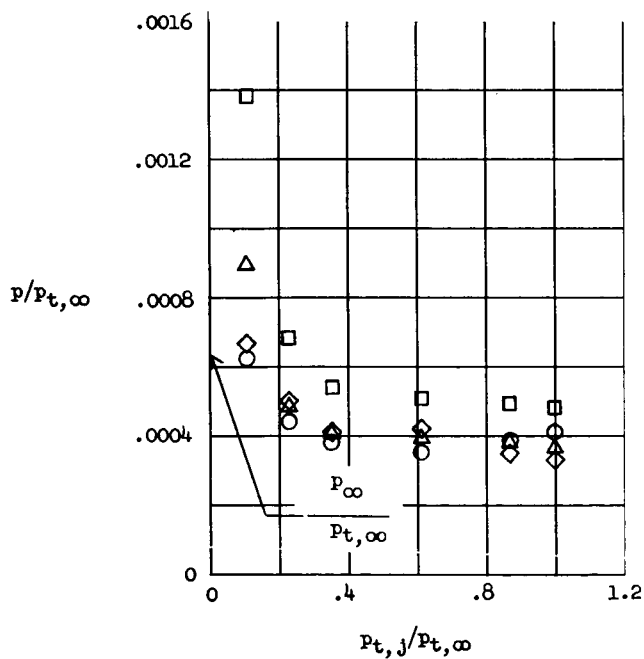
(c) d ≈ 0.01 in. (0.03 cm).

Figure 16.- Surface pressures downstream of jet locations. $M_j = 1.0$.
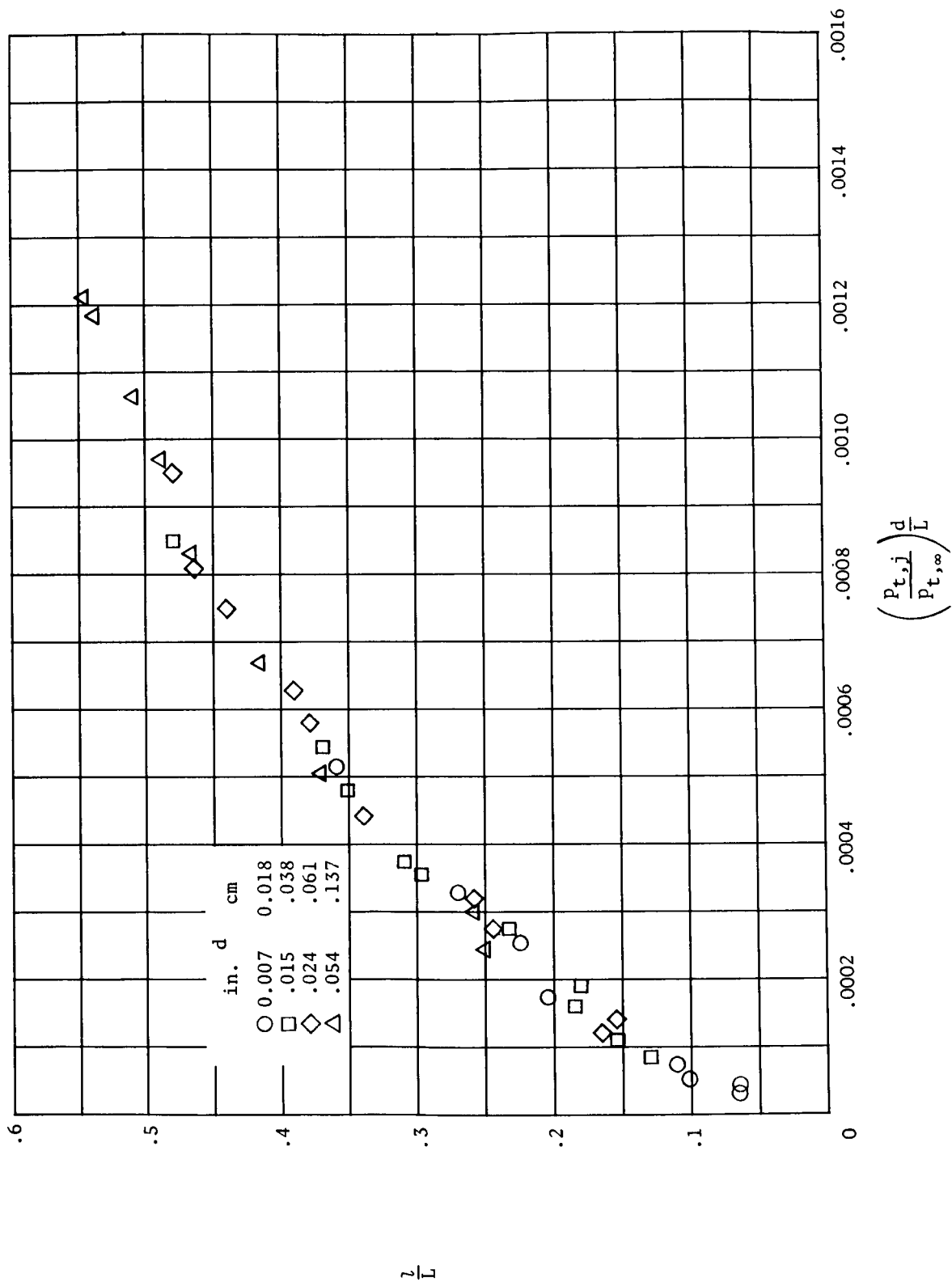
Figure 17.- Effect of mass flow and momentum parameter on separation distances. $M_j = 1.0$.
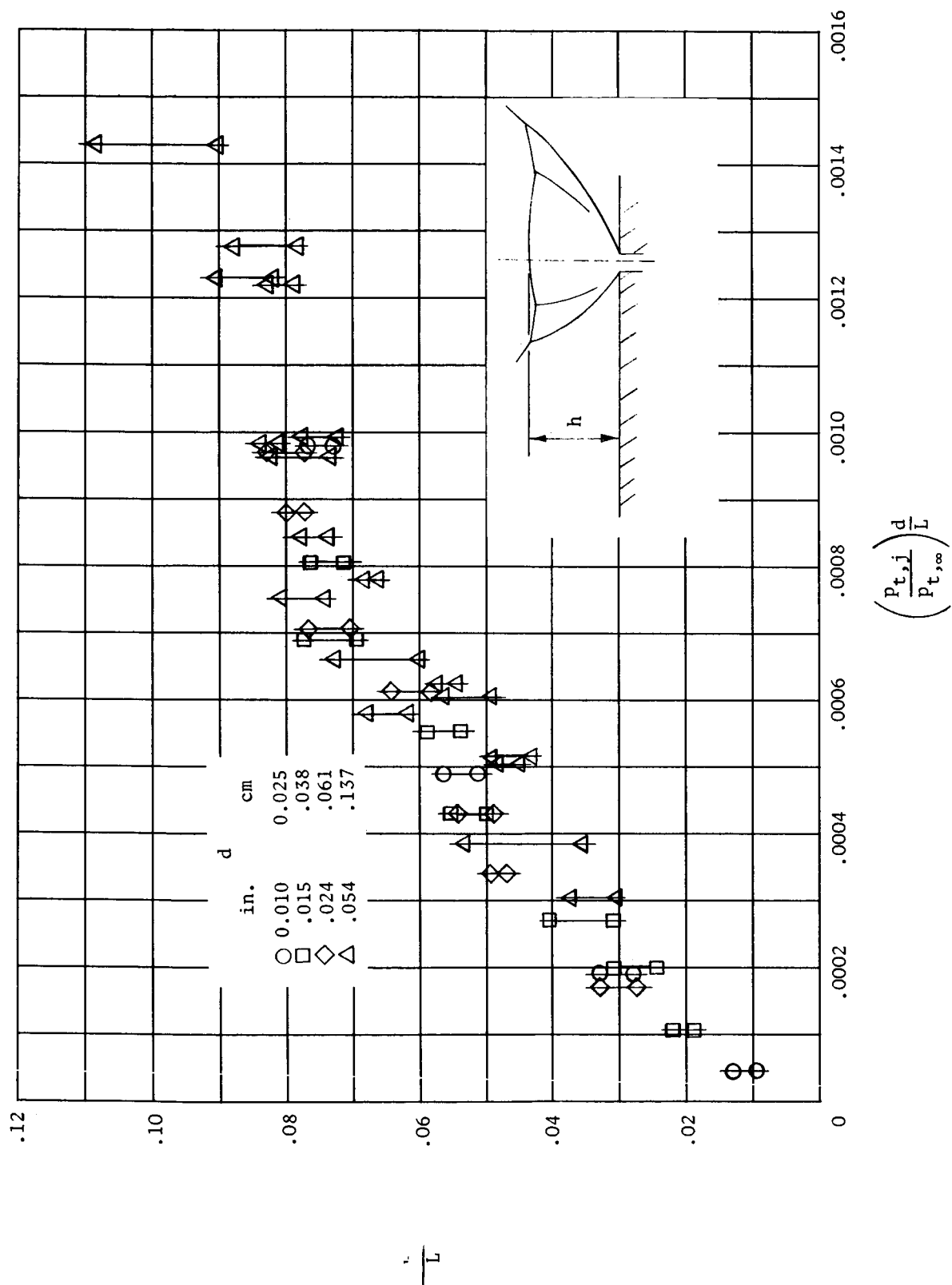
Figure 18.- Effect of mass flow and momentum parameter on jet strong shock height. $M_j = 1.0$.
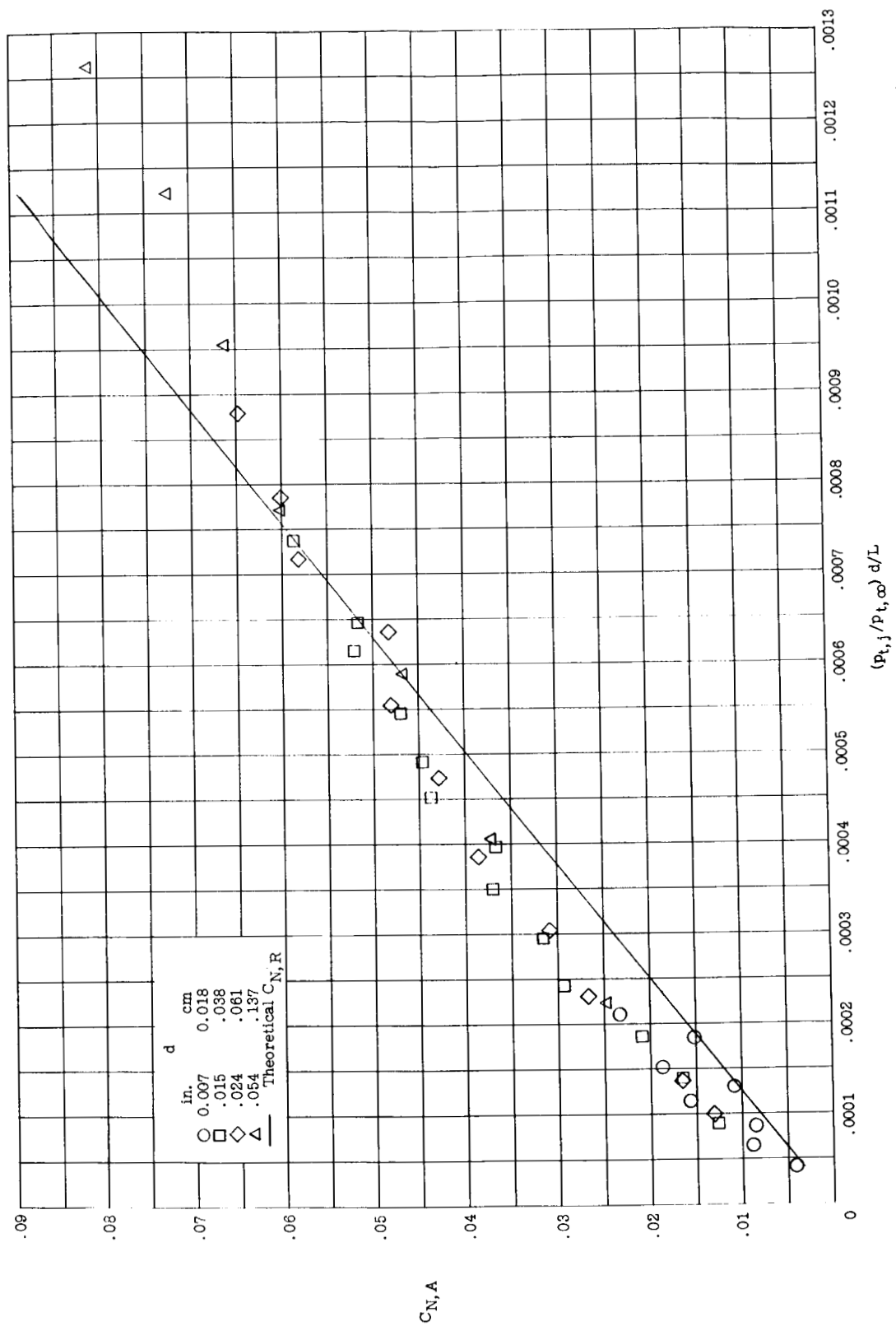
Figure 19.- Effect of jet mass flow and momentum on aerodynamic interaction force coefficient. $M_j = 1.0$.

40
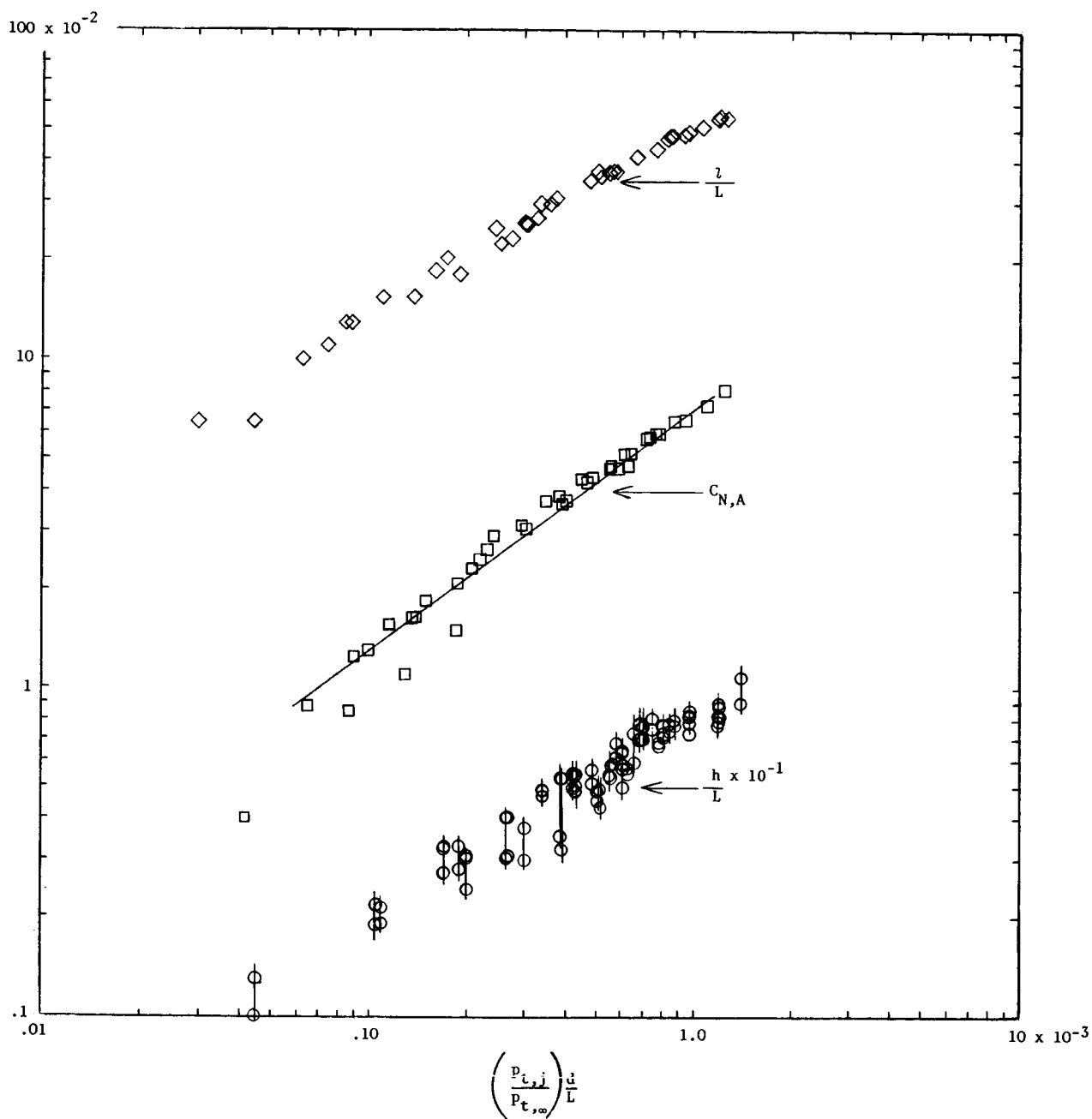
Figure 20.- Comparison of effect of jet mass flow and momentum on jet-induced separation distance, aerodynamic normal force, and jet strong shock height for various slot widths. $M_j = 1.0$.
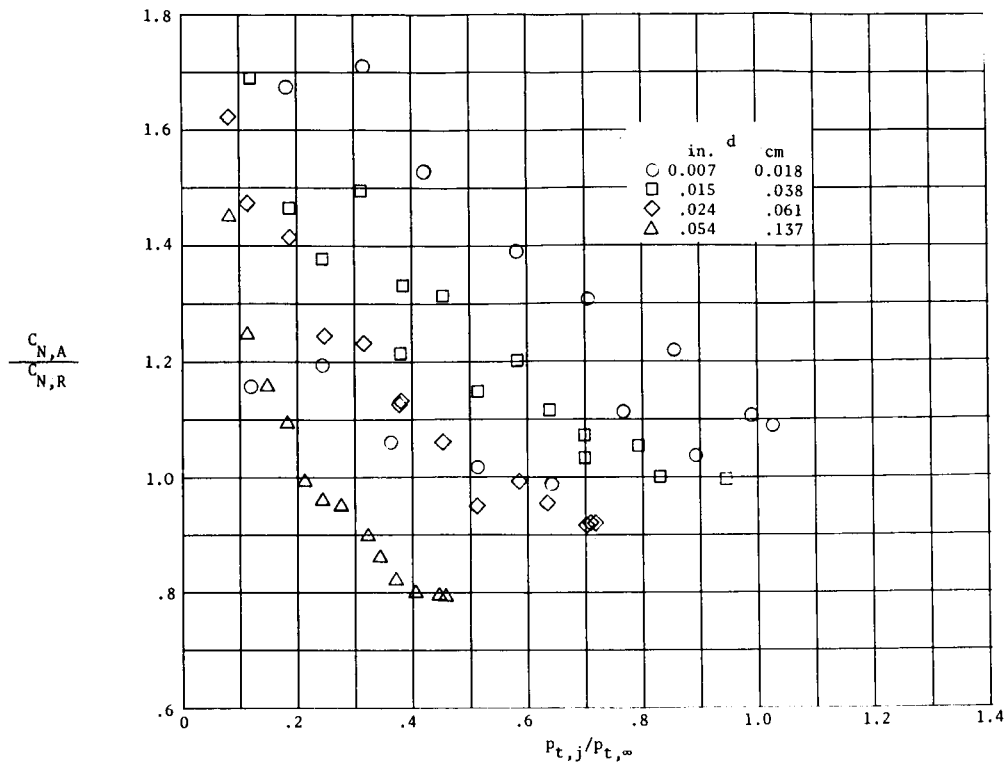
(a) Effect of total pressure ratio on ratio of aerodynamic to reaction normal-force coefficient.
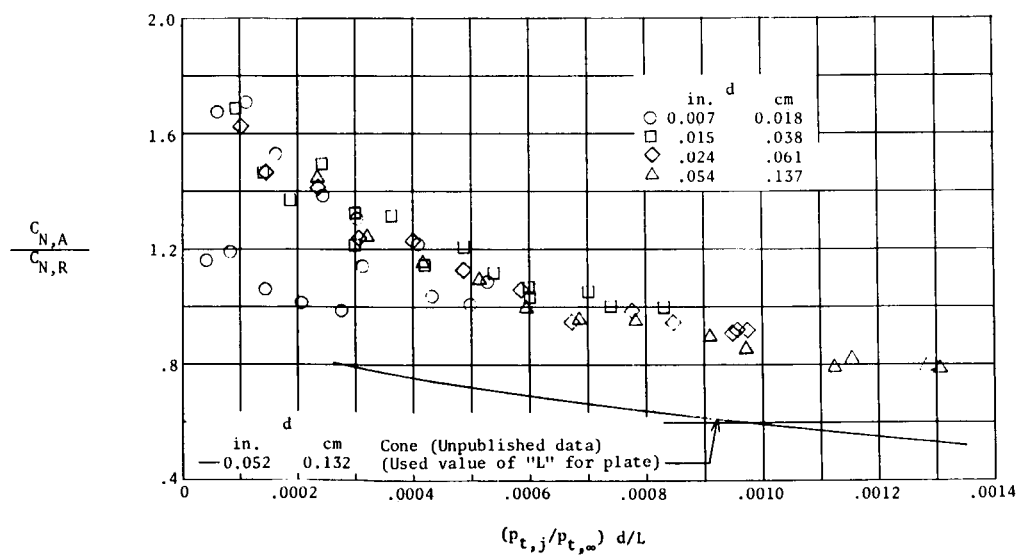
(b) Effect of jet mass flow and momentum on ratio of aerodynamic to reaction normal-force coefficient.

Figure 21.- Effect of various jet parameters on ratio of aerodynamic to reaction normal-force coefficient. $M_j = 1.0$.
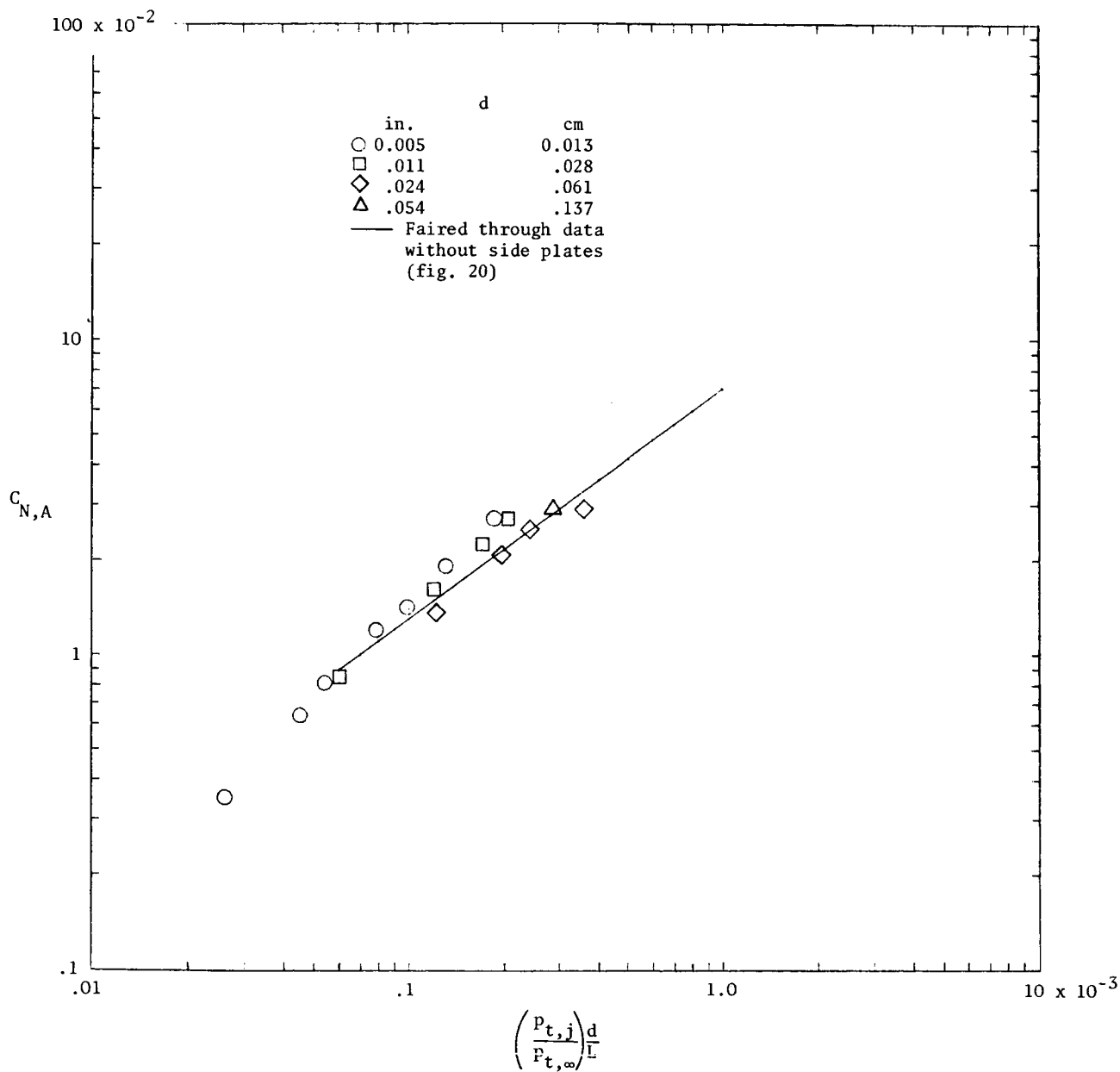
Figure 22.- Effect of jet mass flow and momentum on aerodynamic interaction force coefficients with side plates. $M_j = 1.0$.
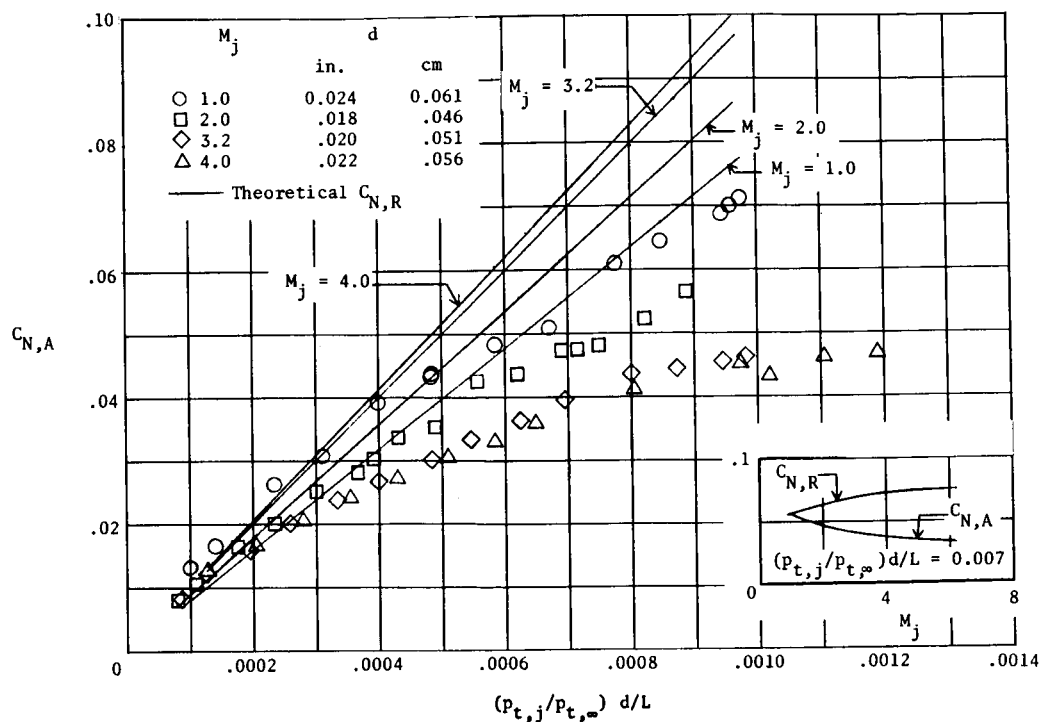
(a) $d \approx 0.020$ in. (0.051 cm).
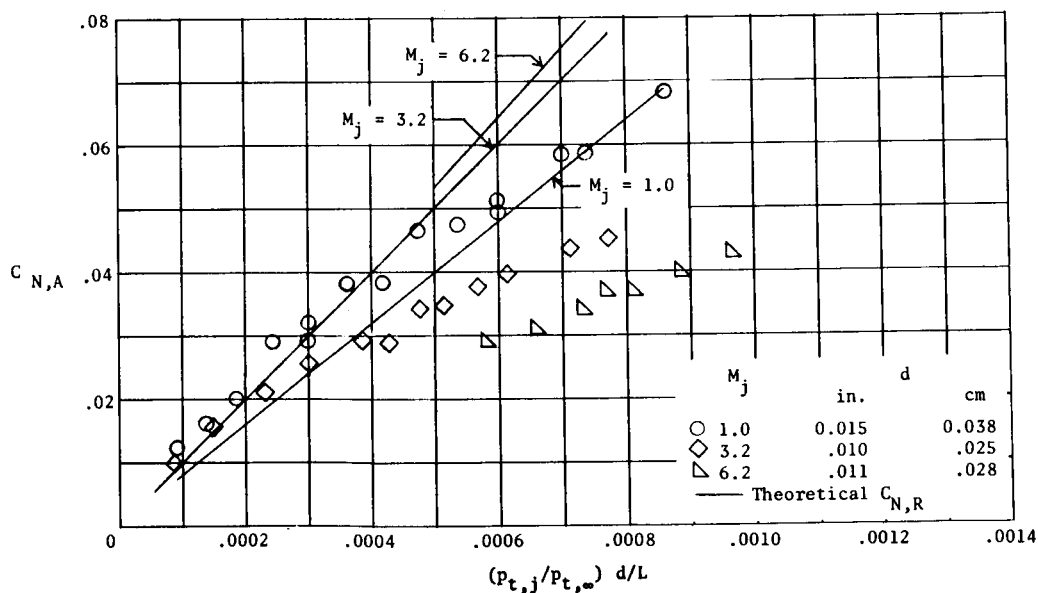
(b) $d \approx 0.010$ in. (0.025 cm).

Figure 23.- Effect of jet mass flow on aerodynamic interaction normal force for various jet Mach numbers.
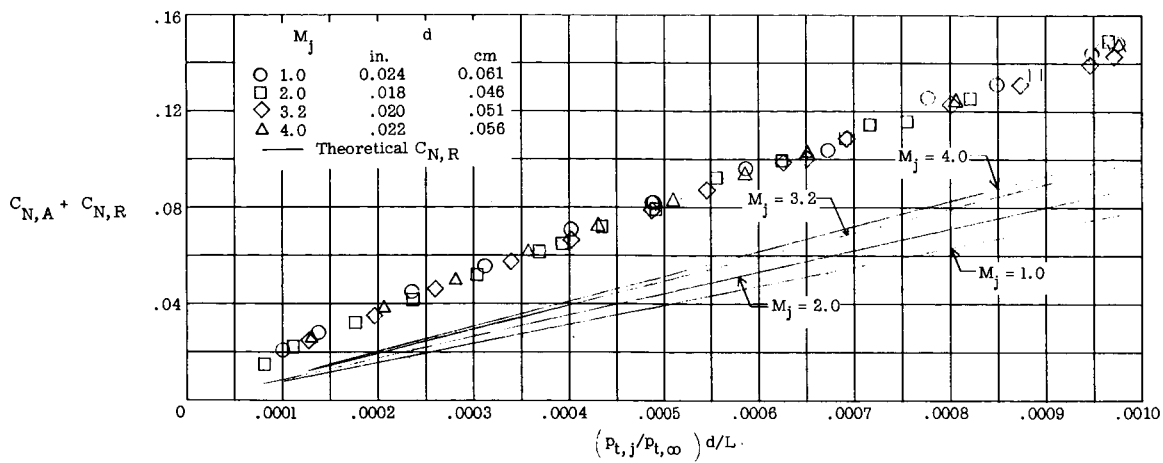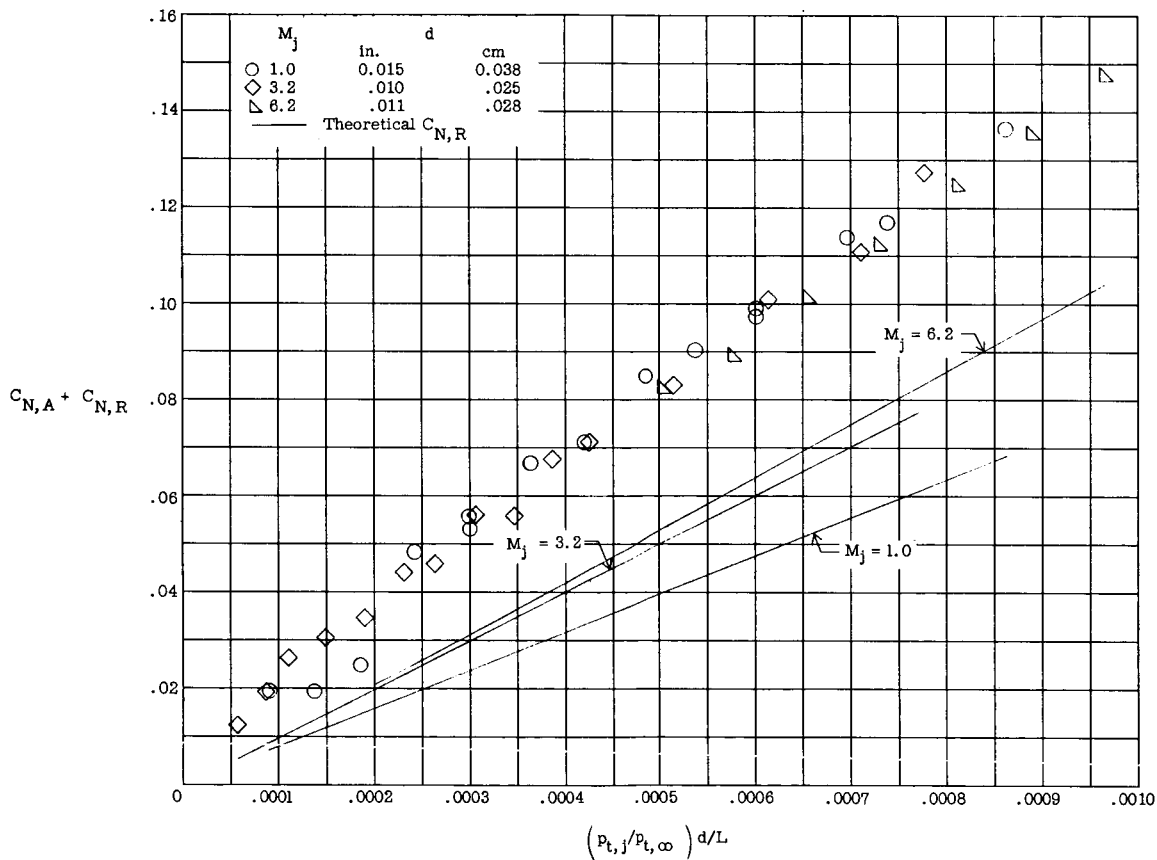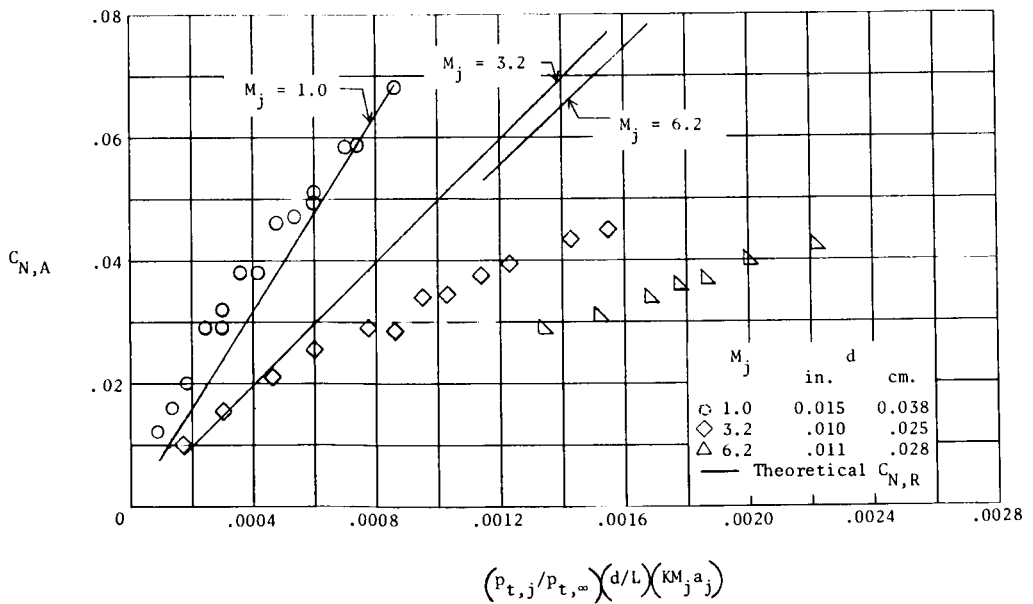
(a) $d \approx 0.020$ in. (0.051 cm).

(b) $d \approx 0.010$ in. (0.025 cm).

Figure 24.- Effect of jet mass flow on total normal force for various jet Mach numbers.
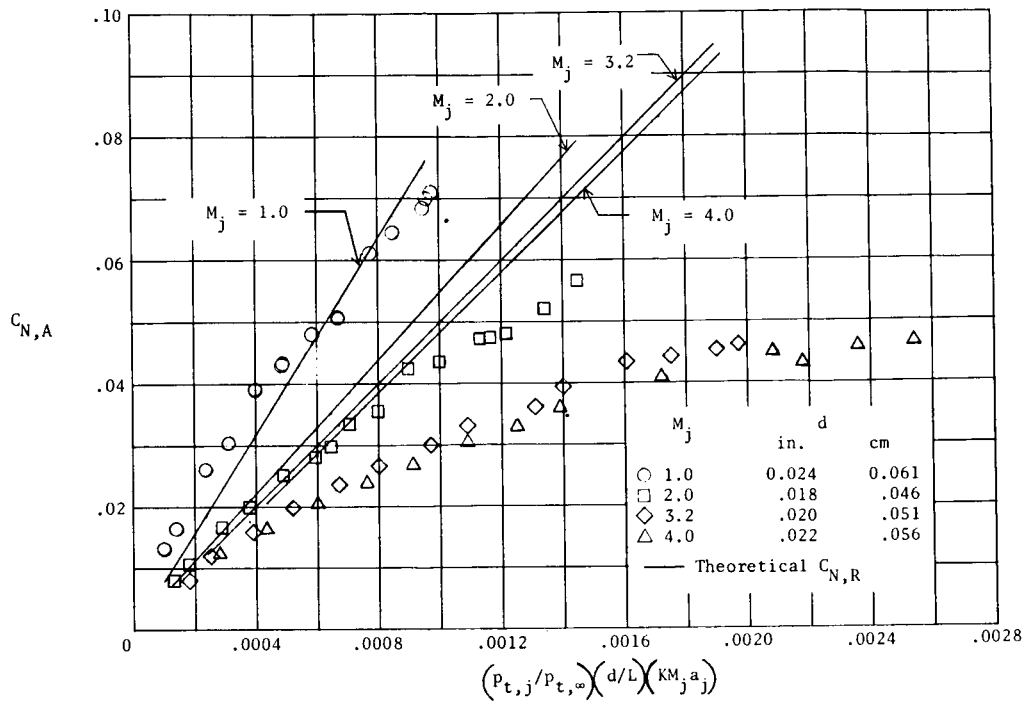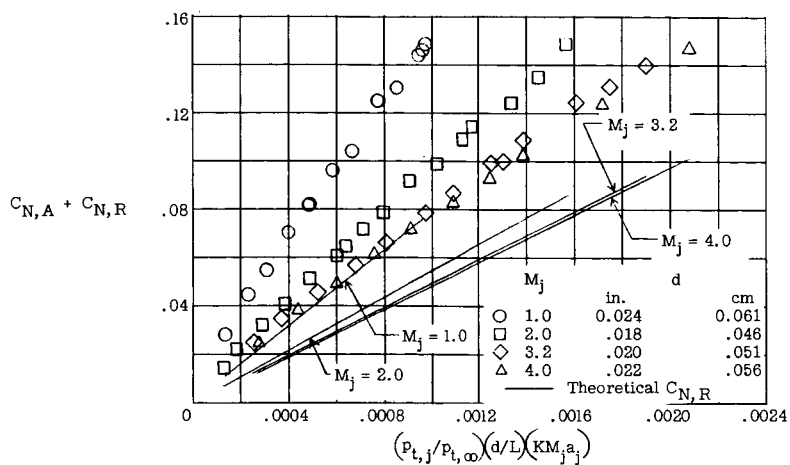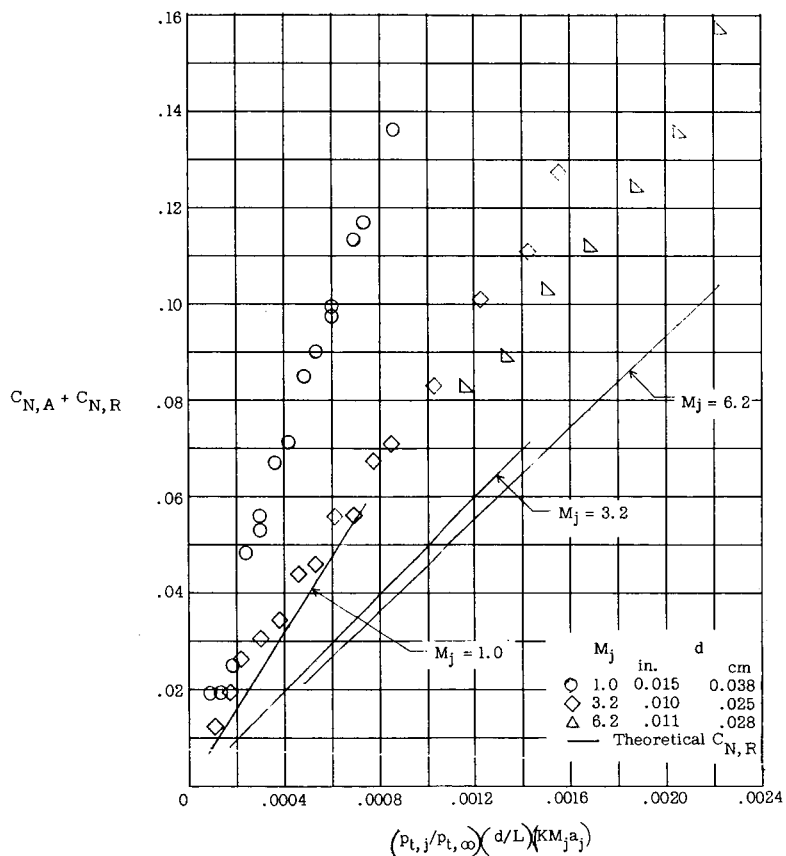
(a) $d \approx 0.020$ in. (0.051 cm).

(b) $d \approx 0.010$ in. (0.025 cm).

Figure 25.- Effect of jet momentum on aerodynamic interaction normal force for various jet Mach numbers.
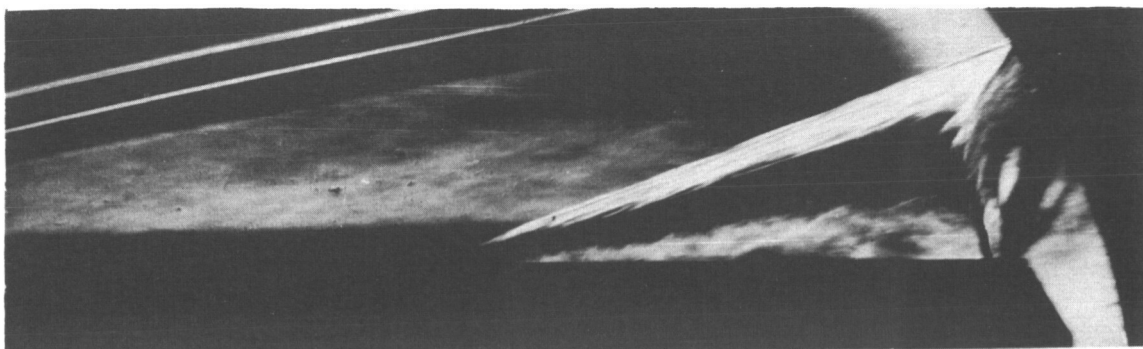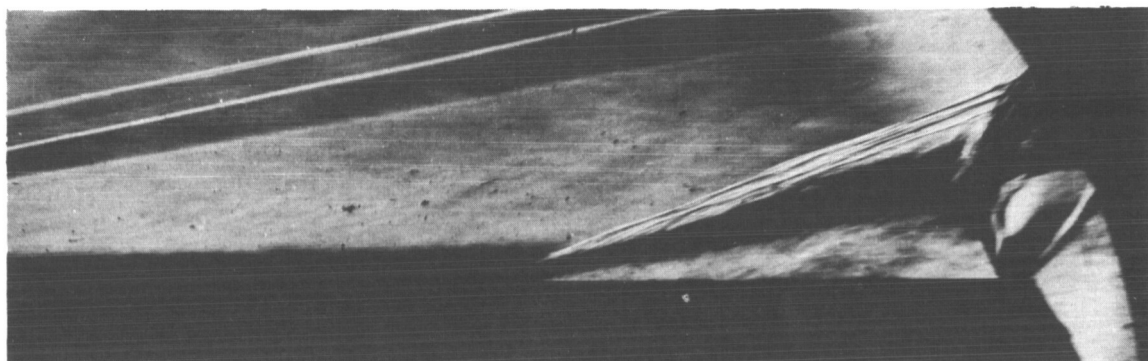
(a) $d \approx 0.020$ in. (0.051 cm).

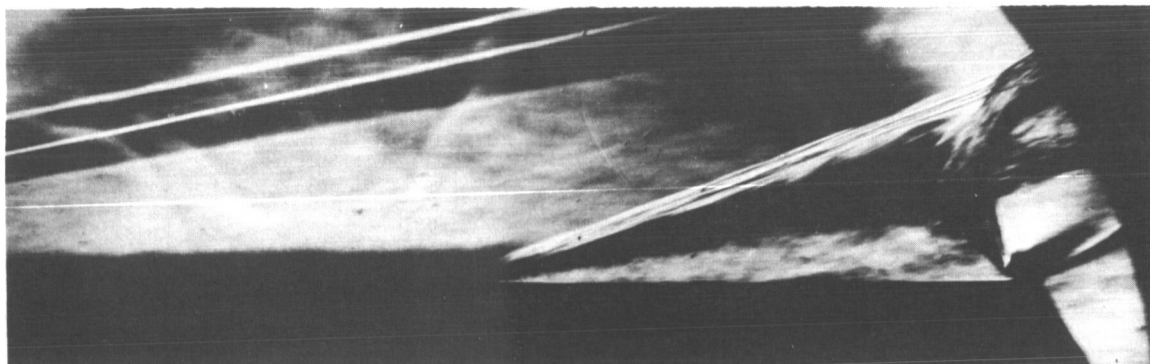(b) $d \approx 0.010$ in. (0.025 cm).

Figure 26.- Effect of jet momentum on total normal force for various jet Mach numbers.

(a) $M_j = 4.0$; $\frac{p_{t,j}}{p_{t,\infty}} = 0.70$; $d = 0.022$ in. (0.05588 cm).

(b) $M_j = 3.2$; $\frac{p_{t,j}}{p_{t,\infty}} = 0.64$; $d = 0.020$ in. (0.05080 cm).

(c) $M_j = 2.0$; $\frac{p_{t,j}}{p_{t,\infty}} = 0.74$; $d = 0.018$ in. (0.04572 cm).

Figure 27.- Typical schlieren photographs. $M_j > 1.0$.

L-66-7603

"The aeronautical and space activities of the United States shall be conducted so as to contribute . . . to the expansion of human knowledge of phenomena in the atmosphere and space. The Administration shall provide for the widest practicable and appropriate dissemination of information concerning its activities and the results thereof."

—NATIONAL AERONAUTICS AND SPACE ACT OF 1958

NASA SCIENTIFIC AND TECHNICAL PUBLICATIONS

TECHNICAL REPORTS: Scientific and technical information considered important, complete, and a lasting contribution to existing knowledge.

TECHNICAL NOTES: Information less broad in scope but nevertheless of importance as a contribution to existing knowledge.

TECHNICAL MEMORANDUMS: Information receiving limited distribution because of preliminary data, security classification, or other reasons.

CONTRACTOR REPORTS: Technical information generated in connection with a NASA contract or grant and released under NASA auspices.

TECHNICAL TRANSLATIONS: Information published in a foreign language considered to merit NASA distribution in English.

TECHNICAL REPRINTS: Information derived from NASA activities and initially published in the form of journal articles.

SPECIAL PUBLICATIONS: Information derived from or of value to NASA activities but not necessarily reporting the results of individual NASA-programmed scientific efforts. Publications include conference proceedings, monographs, data compilations, handbooks, sourcebooks, and special bibliographies.

Details on the availability of these publications may be obtained from:

SCIENTIFIC AND TECHNICAL INFORMATION DIVISION

NATIONAL AERONAUTICS AND SPACE ADMINISTRATION
Washington, D.C. 20546